Journal of Pathology
J Pathol 2021; **00:** 000–000
Published online 18 March 2021 in Wiley Online Library
(wileyonlinelibrary.com) DOI: 10.1002/path.5643

ORIGINAL PAPER

Dual proteotoxic stress accelerates liver injury via activation of p62–Nrf2

Deniz Kuscuoglu[1], Lisa Bewersdorf[1], Kathrin Wenzel[1], Annika Gross[1], Gökce Kobazi Ensari[1], Yizhao Luo[1], Konrad Kilic[1], Kanishka Hittatiya[2], Nicole Golob-Schwarzl[3], Rudolf E Leube[4], Christian Preisinger[5], Jacob George[6], Mayada Metwally[6], Mohammed Eslam[6], Pietro Lampertico[7], Salvatore Petta[8], Alessandra Mangia[9], Thomas Berg[10], Andre Boonstra[11], Willem P Brouwer[11], Maria Lorena Abate[12], Alessandro Loglio[7], Angela Sutton[13,14,15], Pierre Nahon[16,17,18], Benedikt Schaefer[19], Heinz Zoller[19], Elmar Aigner[20], Christian Trautwein[1], Johannes Haybaeck[21,22] and Pavel Strnad[1]*

[1] *Department of Medicine III, University Hospital Aachen, Aachen, Germany*
[2] *Institute of Pathology, University Hospital Bonn, Bonn, Germany*
[3] *Institute of Dermatology, University Hospital Graz, Graz, Austria*
[4] *Institute of Molecular and Cellular Anatomy, RWTH Aachen University, Aachen, Germany*
[5] *Proteomics Facility, Interdisciplinary Centre for Clinical Research (IZKF), Medical School, RWTH Aachen University, Aachen, Germany*
[6] *Storr Liver Centre, Westmead Institute for Medical Research, Westmead Hospital and University of Sydney, Sydney, Australia*
[7] *CRC 'A. M. e A. Migliavacca' Center for Liver Disease Division of Gastroenterology and Hepatology Fondazione IRCCS Ca' Granda – Ospedale Maggiore Policlinico, Università di Milano, Milan, Italy*
[8] *Sezione di Gastroenterologia e Epatologia, DiBiMIS, University of Palermo, Palermo, Italy*
[9] *Division of Hepatology, Ospedale Casa Sollievo della Sofferenza, IRCCS, San Giovanni Rotondo, Italy*
[10] *Section of Hepatology, Clinic for Gastroenterology and Rheumatology, University Clinic Leipzig, Leipzig, Germany*
[11] *Department of Gastroenterology and Hepatology, Erasmus MC - University Medical Center Rotterdam, Rotterdam, The Netherlands*
[12] *Division of Gastroenterology and Hepatology, Department of Medical Science, University of Turin, Turin, Italy*
[13] *Centre de Ressources Biologiques (Liver Disease Biobank) Groupe Hospitalier Paris, Seine-Saint-Denis, France*
[14] *AP-HP Hôpital Jean Verdier, Service de Biochimie, Bondy, France*
[15] *Inserm U1148, Université Paris 13, Bobigny, France*
[16] *AP-HP, Hôpital Jean Verdier, Service d'Hépatologie, Bondy, France*
[17] *Université Paris 13, Sorbonne Paris Cité, 'Equipe Labellisée Ligue Contre le Cancer', Saint-Denis, France*
[18] *Inserm, UMR-1162, 'Génomique Fonctionnelle des Tumeur Solides', Paris, France*
[19] *Department of Internal Medicine I, Medical University of Innsbruck, Innsbruck, Austria*
[20] *First Department of Medicine, Paracelsus Medical University, Salzburg, Austria*
[21] *Department of Pathology, Medical Faculty, Otto-von-Guericke University Magdeburg, Magdeburg, Germany*
[22] *Department of Pathology, Neuropathology and Molecular Pathology, Medical University of Innsbruck, Innsbruck, Austria*

*Correspondence to: P Strnad, Department of Internal Medicine III, RWTH Aachen, Pauwelsstraße 30, D-52074 Aachen, Germany.
E-mail: pstrnad@ukaachen.de

Abstract

Protein accumulation is the hallmark of various neuronal, muscular, and other human disorders. It is also often seen in the liver as a major protein-secretory organ. For example, aggregation of mutated alpha1-antitrypsin (AAT), referred to as PiZ, is a characteristic feature of AAT deficiency, whereas retention of hepatitis B surface protein (HBs) is found in chronic hepatitis B (CHB) infection. We investigated the interaction of both proteotoxic stresses in humans and mice. Animals overexpressing both PiZ and HBs (HBs-PiZ mice) had greater liver injury, steatosis, and fibrosis. Later they exhibited higher hepatocellular carcinoma load and a more aggressive tumor subtype. Although PiZ and HBs displayed differing solubility properties and distinct distribution patterns, HBs-PiZ animals manifested retention of AAT/HBs in the degradatory pathway and a marked accumulation of the autophagy adaptor p62. Isolation of p62-containing particles revealed retained HBs/AAT and the lipophagy adapter perilipin-2. p62 build-up led to activation of the p62–Nrf2 axis and emergence of reactive oxygen species. Our results demonstrate that the simultaneous presence of two prevalent proteotoxic stresses promotes the development of liver injury due to protein retention and activation of the p62–Nrf2 axis. In humans, the PiZ variant was over-represented in CHB patients with advanced liver fibrosis (unadjusted odds ratio = 9.92 [1.15–85.39]). Current siRNA approaches targeting HBs/AAT should be considered for these individuals.
© 2021 The Authors. *The Journal of Pathology* published by John Wiley & Sons, Ltd. on behalf of The Pathological Society of Great Britain and Ireland.

Keywords: aggregate; inclusion; lipophagy; SERPINA1; oxidative stress; cirrhosis

Received 29 March 2020; Revised 29 January 2021; Accepted 10 February 2021

No conflicts of interest were declared.

© 2021 The Authors. *The Journal of Pathology* published by John Wiley & Sons, Ltd. on behalf of The Pathological Society of Great Britain and Ireland. This is an open access article under the terms of the Creative Commons Attribution-NonCommercial-NoDerivs License, which permits use and distribution in any medium, provided the original work is properly cited, the use is non-commercial and no modifications or adaptations are made.

Introduction

Accumulation of damaged proteins is a characteristic hallmark of various human diseases, including neurodegenerative, muscular, and other disorders [1]. Hepatocytes are among the most proteostatically challenged cells, as they produce the majority of serum proteins [2,3]. Serum proteins are synthesized in the ER and processed by the Golgi apparatus before being secreted into the bloodstream. Protein folding and quality control in the ER is facilitated by chaperones such as the calnexin–calreticulin system or BiP [4]. Proteins that cannot be folded properly are degraded by the proteasome or the autophagic machinery [5]. An inability to cope with the tremendous protein flow-through leads to the emergence of protein aggregates that constitute a hallmark of multiple chronic liver diseases [2]. The best-known examples include an inherited disorder, alpha1-antitrypsin (AAT) deficiency [6,7], as well as chronic hepatitis B (CHB) infection [2,3]. The former is caused by mutations in the *AAT* (*SERPINA1*) gene that lead to a rapid polymerization and retention of the mutant protein in hepatocytes. It results in characteristic roundish aggregates that are detected by PAS-D staining [2,8]. For the latter, an unbalanced production of the large isoform of the hepatitis B surface protein (HBs) leads to its accumulation in the ER, giving rise to ground glass hepatocytes [2].

AAT deficiency constitutes the third most common lethal genetic disorder [2,9–11]. In northern Europe, up to 1:2000 is homozygous for the characteristic, disease-causing variant termed PiZ [9]. While the presence of the homozygous PiZ mutation (referred to as PiZZ) precipitates the development of liver disease [12], the heterozygous PiZ carriage (PiMZ), which has a prevalence of up to 20% in northern Europe, is a well-established disease modifier [13]. For example, the heterozygous PiZ carriage predisposes patients with cystic fibrosis to the development of severe liver disease [14] and a large genome-wide study identified PiZ as the variant conferring the highest odds for alcoholic liver disease/non-alcoholic fatty liver disease (ALD/NAFLD)-associated liver cirrhosis [15]. Although the importance of PiZ for the progression of ALD/NAFLD-related liver disease has been firmly established [15,16], only cohorts with limited size have addressed its relevance in other disorders such as hemochromatosis or chronic viral hepatitis [2]. Accordingly, a small study reported a high prevalence of hepatitis B infection among patients with heterozygous PiZ mutations, and the infected PiZ carriers often had advanced liver disease [17]. Beyond human association studies, transgenic mice overexpressing PiZ are used as an experimental tool to study the biological consequences of PiZ production. These animals form the characteristic AAT globules and display chronic liver injury that is proportional to the amount of overexpressed protein [18,19]. Similar to patients with AAT deficiency, PiZ mice may also develop liver tumors during aging [2,8].

CHB infection is the main risk for the development of hepatocellular carcinoma (HCC) [20]. Although treatment with nucleoside/nucleotide analogs effectively suppresses viral replication, it does not completely prevent the progression of the disease, thereby pointing to a direct damaging role of viral DNA that is integrated into the genome of the host and leads to production of viral proteins [21]. Among them, HBs has received particular attention. The hepatitis B S-gene (*HBs*) gives rise to three surface (envelope) proteins, i.e. the small (S), the middle (pre-S2 and S), and the large surface protein (pre-S1, pre-S2, and S). The excess formation of large surface protein as caused by mutations in the *HBs* gene leads to the formation of filamentous particles that are confined in the ER [2]. Several studies have shown that subjects with high HBs serum levels display an increased risk of HCC [22,23]. To directly address the impact of this protein on the development of liver damage, mice overexpressing the large surface protein (HBs mice) were generated [24], and were shown to develop chronic liver injury, as well as liver tumors later in their lives [25,26].

Despite the undisputed importance of the proteostatic challenge in the development of liver disease, the crosstalk between the different stresses and the exact molecular mechanisms leading to liver injury remain largely unknown. This is remarkable as siRNA drugs silencing both HBs and AAT are entering clinical trials. Therefore, to study the clinical relevance of dual proteotoxic stress, we screened a large cohort of patients with CHB for the presence of the PiZ variant. Moreover, we crossbred animals overexpressing PiZ with HBs-overexpressing animals. In both patients and transgenic animals, the simultaneous production of both proteins promoted the development of liver disease, and in mice, an accelerated hepatocarcinogenesis was noted. We observed a retention of proteins with subsequent activation of the p62-Nrf2 axis as a probable underlying mechanism.

Materials and methods

Human subjects

Tissue samples for molecular analyses were obtained from 12 patients who underwent a liver biopsy at the universities of Aachen, Bonn, Innsbruck, and Salzburg (see supplementary material, Table S1). Tissues were cut in half and either used for histological staining or were frozen for immunofluorescence/biochemical analysis. Patients were excluded if they: (1) had evidence of co-infection with either hepatitis C virus, hepatitis delta virus or human immunodeficiency virus, (2) were diagnosed with or suspected to have HCC or alpha-fetoprotein >100 ng/ml, or (3) had evidence of other liver diseases by standard tests. Patients with hepatic decompensation defined as: (1) ascites (overt or by ultrasound), (2) hepatic encephalopathy, (3) gastroesophageal variceal bleeding, (4) jaundice or (5) hepatorenal syndrome were excluded. Liver histopathology was scored by expert pathologists according to METAVIR [27].

© 2021 The Authors. *The Journal of Pathology* published by John Wiley & Sons, Ltd. on behalf of The Pathological Society of Great Britain and Ireland. www.pathsoc.org

Fibrosis was staged from F0 (no cirrhosis) to F4 (cirrhosis).

Patients with CHB (830) of self-reported Caucasian ancestry were analyzed prior to initiation of antiviral therapy (see supplementary material, Table S2). All participants were positive for HBs antigen for at least 6 months, and all underwent a liver biopsy that was used to determine the fibrosis stage. Subsequently, we compared the occurrence of PiZ variant (rs28929474) in patients with no/mild (F0–F2; $n = 542$) and advanced liver fibrosis (F3–F4; $n = 281$). Genotyping was performed using DNA obtained from peripheral blood samples and the TaqMan SNP genotyping allelic discrimination assay (Applied Biosystems, Foster City, CA, USA) and was carried out without knowledge of clinical parameters. Exclusion of comorbidities was carried out as described above. All participant sites had ethics approval from their respective ethics committees. Written informed consent to participate in the study was obtained from all patients, and the analysis was in compliance with the 1975 Declaration of Helsinki. The study was approved by the Human Subjects Committees of the participating centers.

Animal studies

Previously described transgenic mice overexpressing PiZ [18] and HBs (Tg Alb-1HBV) Bri 44 [24] had been crossbred to obtain animals overexpressing both proteins (Z-HBs mice). The mice were sacrificed at the age of 2, 10, and 14 months. The tumors arising in HBs and Z-HBs mice were compared with the tumors obtained in mice treated with diethylnitrosamine (DEN) and carbon tetrachloride (CCl_4), an established model of well-differentiated HCC. For tumor initiation, a single injection of DEN (i.p. injection of 26 µg/g body weight into 14-day-old mice) was administered, followed by repeated tumor growth promotion by dosing with CCl_4 (i.p. injection of 0.5 µl/g body weight once every week, dissolved in seed oil, starting 2 weeks after the DEN treatment) for 22 weeks. The mice were sacrificed at the age of 26 weeks, 2 weeks after the last CCl_4 dose. All animals were kept in 12-h dark–light cycles in the RWTH's animal housing with standard feed (Ssniff, Soest, Germany) and were fasted for 10–12 h prior to sacrifice via overdose of isoflurane (Abbvie, Maidenhead, UK). Serum collection and liver tissue dissection were as described previously [28]. Serum levels of liver enzymes, AAT (immunonephelometric assay; BNII/BN Prospec System, Siemens, Marburg, Germany) and HBs levels (Elecsys HBs Ag II, Roche Diagnostics, Mannheim, Germany) were measured by the Clinical Chemistry Department, University Hospital Aachen. Macroscopically visible tumors were cut into pieces and placed in 10% formaldehyde (for histological staining), snap frozen in liquid nitrogen (for biochemical analyses) or submerged in RNAlater stabilization reagent (Ambion, Life Technologies, Darmstadt, Germany). Animal experiments were approved by the responsible authority of the state North-Rhine-Westphalia (LANUV) and were carried out in accordance with the German Law for Welfare of Laboratory Animals.

Statistical analyses

All statistical analyses were performed using GraphPad Prism 5 software (GraphPad, San Diego, CA, USA). The Kolmogorov–Smirnoff test was used to determine the normality of distribution. For normally distributed samples, the data are presented as mean ± SEM, and a parametric one-way ANOVA analysis was applied. For samples that were not normally distributed, a non-parametric ANOVA with Kruskal–Wallis *post hoc* test was carried out. The frequency of PiZ variants in patients with mild versus advanced liver fibrosis was assessed using a chi-squared test. Binary logistic regression was used to calculate odds ratios. Two-sided P values below 0.05 were considered statistically significant.

Details for tissue staining, electron microscopy, RT-qPCR analysis, protein analysis, biochemical assays and LC3 flux assays are presented in supplementary material, Supplementary materials and methods.

Results

PiZ and HBs display differing distribution and solubility properties

To determine the relationship between the retention of PiZ and HBs, we analyzed CHB patients with/without a simultaneous presence of PiZ variant as well as non-infected individuals harboring PiZ (Figure 1A, supplementary material, Table S1). Immunohistochemical and immunofluorescence staining revealed a differing protein distribution pattern: more evenly distributed, cloudy staining in the case of HBs and well-demarcated, roundish, clustered, and unequally dispersed bodies in the case of AAT. The accumulation of both proteins was not markedly altered in individuals harboring both PiZ and HBs (Figure 1B). Biochemical analysis revealed varying solubility properties: PiZ is largely insoluble in non-ionic detergents, whereas HBs and the non-mutated AAT are located almost exclusively in the soluble fraction (Figure 1C).

Two-month-old PiZ-HBs mice demonstrate stronger liver injury, smaller AAT globules, and a shift of HBs from the soluble to insoluble pool

To evaluate the consequences of simultaneous retention of both proteins, we crossed PiZ mice with mice overexpressing the large isoform of HBs. All transgenic mice were viable and developed normally (see supplementary material, Figure S1A). At 2 months of age, Z-HBs mice exhibited mildly elevated levels of transaminases and alkaline phosphatase that were, however, significantly higher than the levels seen in the other genotypes

© 2021 The Authors. *The Journal of Pathology* published by John Wiley & Sons, Ltd. on behalf of The Pathological Society of Great Britain and Ireland. www.pathsoc.org

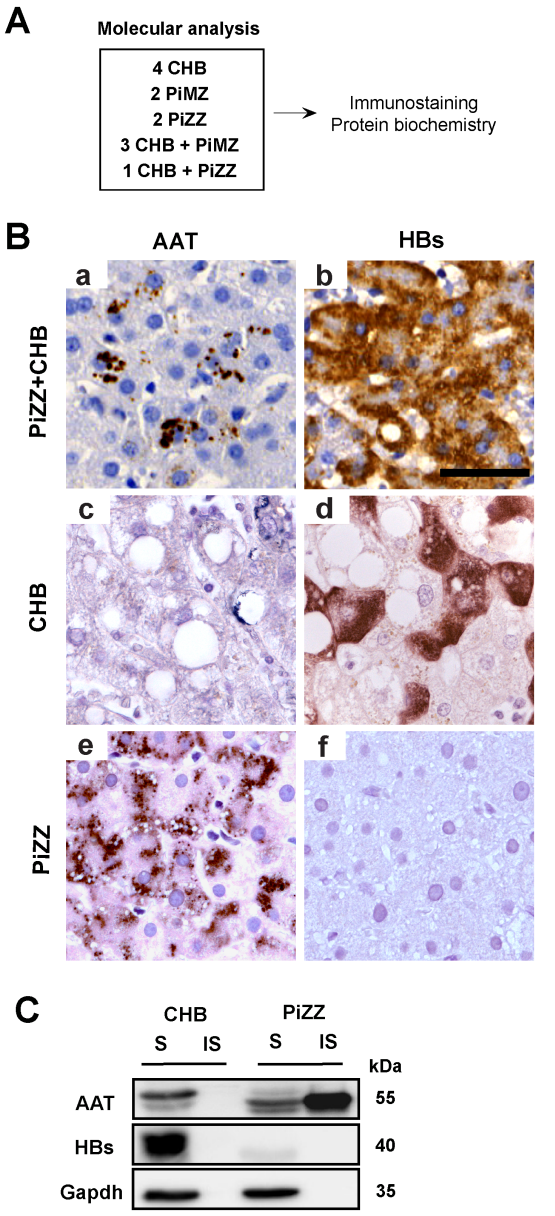


Figure 1. Interaction between the HBs produced during CHB and the mutant PiZ variant of AAT. (A) A schematic of the cohort of 12 patients used for the molecular analysis. PiMZ/PiZZ refers to the presence of heterozygous/homozygous PiZ mutation. (B) Immunohistochemistry reveals PiZ and HBs signals in a patient with CHB only (CHB), a patient with homozygous PiZ mutation (PiZZ) only and a CHB patient carrying a homozygous PiZ mutation (patient PiZZ+CHB). Scale bar, 50 µm (B, b). (C) Immunoblotting demonstrates the solubility of PiZ and HBs in 1% Triton X buffer. Fractionation into a soluble (S) and insoluble pool (IS) is shown for a PiZZ patient without CHB (PiZZ) and in an individual with CHB without the presence of PiZ (CHB). GAPDH, a well-established soluble protein, was used as the loading control.

(Figure 2A). Histological changes were rather modest with discrete inflammation (Figure 2B; supplementary material, Table S3). In addition, a more pronounced accumulation of lipid droplets (Figure 2B,C), as well as an increase in hepatic triglyceride content (Figure 2D), was noted in Z-HBs mice. As a potential mechanistic explanation for the steatosis phenotype, double transgenic animals displayed markedly increased levels of perilipin-2 (Plin2), which is known to protect lipid droplets from lipolysis (Figure 2E,F) [29,30]. Notably, Plin2 accumulation occurred on a post-transcriptional level, because its mRNA levels were similar in all genotypes (see supplementary material, Figure S1B). No significant changes in serum lipid parameters were observed, suggesting that the steatosis was not due to impaired lipid secretion (see supplementary material, Figure S1C).

The simultaneous expression of HBs and AAT affected neither the hepatic levels of both proteins (see supplementary material, Figure S2A,B) nor their secretion, as demonstrated by comparable serum levels (see supplementary material, Figure S2C). On the other hand, HBs mRNA expression was somewhat lower in Z-HBs mice compared with HBs animals, whereas no changes were observed in AAT mRNA level (see supplementary material, Figure S2D). In line with human findings, AAT was insoluble in non-ionic detergents, whereas HBs was predominantly soluble (see supplementary material, Figure S2E,F). Immunofluorescence revealed a distinct, non-overlapping pattern of AAT and HBs signals (see supplementary material, Figure S3A). Of note, PiZ inclusions in Z-HBs mice were markedly smaller but more frequent (see supplementary material, Figure S3B,C). Ultrastructural analysis revealed similar, irregularly shaped PiZ bodies in mice of both genotypes (see supplementary material, Figure S3D), and the inclusions were easily distinguished from smooth, round-shaped lipid vesicles (not shown). To further define the localization of both proteins, we carried out co-staining with the classic ER resident protein calnexin. Calnexin signals displayed a strong co-localization with HBs but not with AAT (see supplementary material, Figure S3E,F). The overlap between HBs and calnexin was less pronounced in Z-HBs mice compared with the single transgenes (see supplementary material, Figure S3Eg,Eh). In line with this, the additional presence of AAT led to a translocation of HBs into the Triton X-insoluble pool, suggesting a retention of misfolded protein (see supplementary material, Figure S2F,G), which was further supported by the discrepancy between mRNA and protein levels.

Ten-month-old double transgenics display accelerated proliferation, liver fibrosis, and stronger dysplastic changes

Compared with 2-month-old animals, 10-month-old double transgenic animals demonstrated higher levels of liver transaminases and alkaline phosphatase (see supplementary material, Figure S4A) and a modest increase in liver-to-body weight ratios (see supplementary material, Figure S4B). The chronic proteotoxic stress induced the development of liver fibrosis that was particularly prominent in Z-HBs mice (Figure 3A–C). In agreement with these findings, Z-HBs mice showed a significant increase in hepatic hydroxyproline content (see supplementary material, Figure S4C). Furthermore, more pronounced dysplastic changes (Figure 3A,D) and a significantly higher

© 2021 The Authors. *The Journal of Pathology* published by John Wiley & Sons, Ltd. on behalf of The Pathological Society of Great Britain and Ireland. www.pathsoc.org

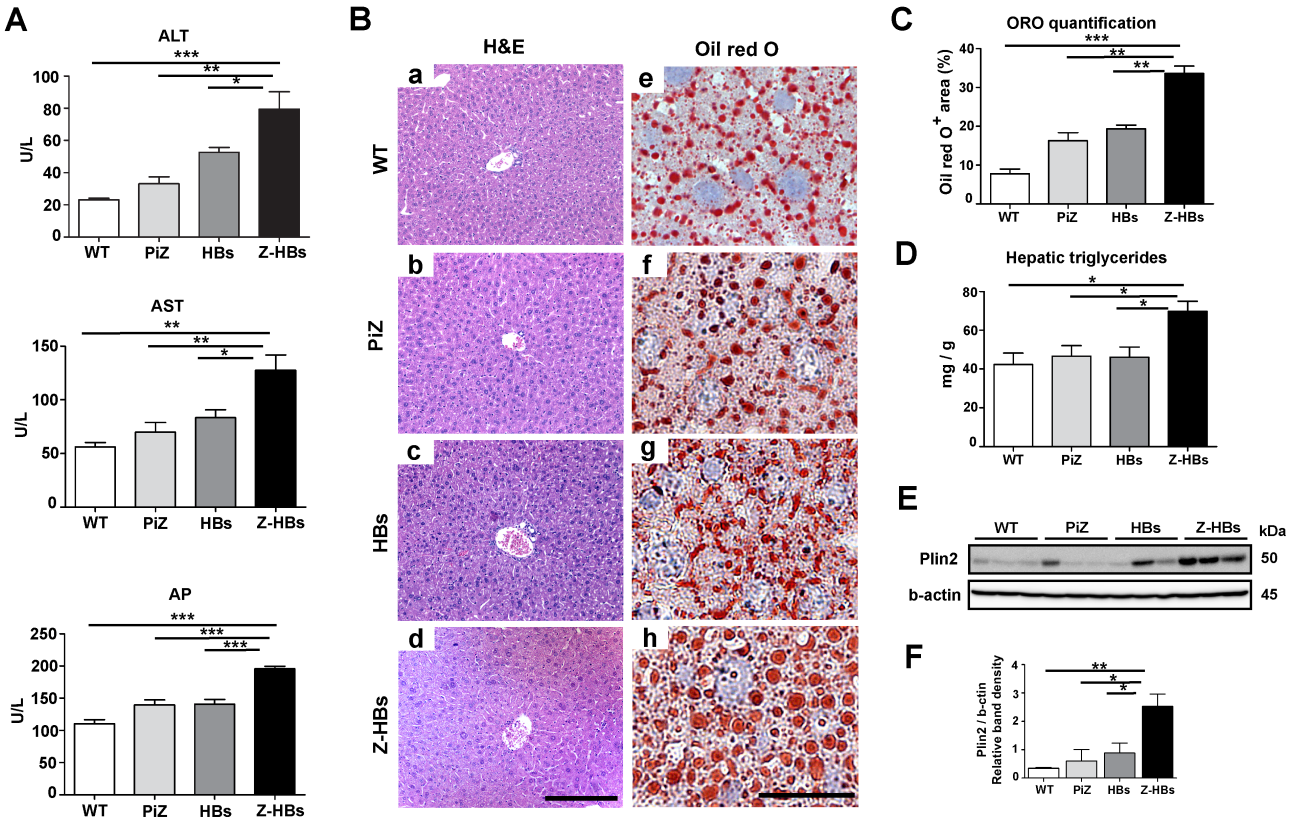


Figure 2. Two-month-old double transgenic animals display significantly greater liver injury and hepatic lipid accumulation. (A) Serum levels of alanine transaminase (ALT), aspartate transaminase (AST) and alkaline phosphatase (AP) were determined in non-transgenic animals (WT) and mice overexpressing HBs, the PiZ variant of AAT (PiZ) or both proteins (Z-HBs). Results are shown as mean ± SEM (n = 5). (B) H&E staining (a–d) reveals the overall liver architecture, whereas Oil-red O (ORO) staining (e–h) with (C) morphometric analysis (mean ± SEM; n = 5) and (D) hepatic triglyceride content (mean ± SEM; n = 10) express the extent of lipid accumulation. Scale bar, 200 µm (d), 25 µm (h). (E) Plin2 protein levels in total liver lysates were determined by immunoblotting. (F) The band density was quantified in relation to b-actin, which was used as a loading control (mean ± SEM; n = 3). $^{*}p \leq 0.05$, $^{**}p \leq 0.01$, $^{***}p \leq 0.001$.

hepatocellular proliferation (Figure 3A,E) were detected by CD44V6 and proliferating cell nuclear antigen (PCNA) immunohistochemical staining, respectively.

Fourteen-month-old mice exhibit increased HCC development

In 14-month-old mice, combined accumulation of both proteins resulted in an increased tumorigenesis that probably contributed to a higher liver-to-body weight ratio (Figure 4A,B; see supplementary material, Figure S5A) and to markedly elevated serum liver injury markers (see supplementary material, Figure S5B). The nodules were significantly larger and more abundant in double transgenic animals (Figure 4B). Although HCC has been consistently observed in aged HBs and Z-HBs mice, PiZ mice showed only sporadic cases (Figure 4B). The tumors dissected from HBs and Z-HBs mice resembled differentiated HCCs (Figure 4C). In line with that, they displayed a preserved or even elevated expression of the hepatocellular genes (see supplementary material, Figure S6A), whereas the cholangiocellular/progenitor lineage markers remained low (see supplementary material, Figure S6B). Notably, a comparable gene expression pattern was seen in tumors induced by a combined treatment with DEN and CCl_4 that constitute an established model of well-differentiated HCCs (see supplementary material, Figure S6C, [31]). Histopathologic examination revealed a trend towards lower apoptosis rates and a significantly lower portal inflammation in tumors dissected from double transgenics (see supplementary material, Table S4). The latter also displayed a higher number of proliferating cells, as illustrated by PCNA staining (Figure 4D,E), and more pronounced DNA damage demonstrated by pγH2AX staining (Figure 4D,E). Gene expression analysis revealed a more aggressive, less differentiated tumor subtype in double transgenic mice, as indicated by downregulation of *Cyp2e1*, *Aqp9*, *Apoc4*, *C1s1*, *Hnf4a*, *Myc*, and *C3* (Figure 4F).

Double transgenic mice harbor an activation of the p62-Nrf2 axis and protein retention in the degradatory pathway

To elucidate the molecular mechanisms leading to a more pronounced liver disease in Z-HBs mice, we concentrated on 2-month-old animals. Despite a trend towards increased IRE1 and CHOP levels (see supplementary material, Figure S7A,B), we did not observe

© 2021 The Authors. *The Journal of Pathology* published by John Wiley & Sons, Ltd. on behalf of The Pathological Society of Great Britain and Ireland. www.pathsoc.org

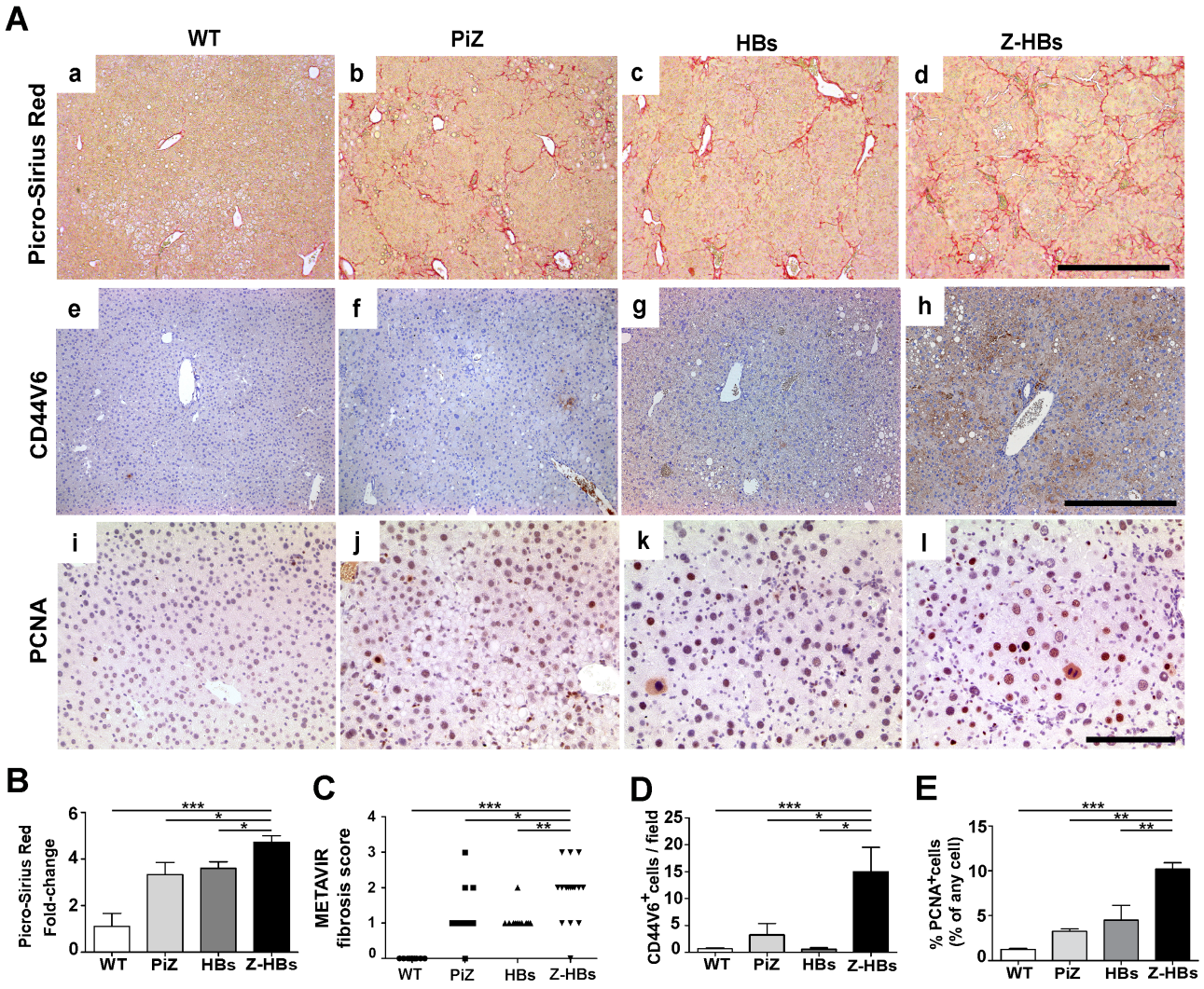


Figure 3. The simultaneous presence of AAT and HBs promotes the development of liver fibrosis in 10-month-old double transgenic mice. (A–C) Picro-Sirius Red staining of liver sections from non-transgenic animals (WT) (a), animals overexpressing PiZ (b), HBs (c) or both proteins together (Z-HBs) (d) with morphometric quantification (B) and evaluation of fibrosis stages with METAVIR score ($n = 6$) (mean ± SEM; $n = 6$). Scale bar, 500 μm (C). For the morphometric evaluation, the average Picro-Sirius Red-positive area in non-transgenic animals was normalized and the areas in other genotypes represent a ratio. (A,D,E) Immunohistochemical staining of liver sections for CD44V6 (A; e–h) and PCNA (A; i–l) with subsequent quantification (D,E). Scale bar, 500 μm (d), 200 μm (h). Results are expressed as mean ± SEM ($n = 4$–6). $^{*}p \leq 0.05$, $^{**}p \leq 0.01$, $^{***}p \leq 0.001$.

an obvious activation of an unfolded protein response. In particular, BiP or ATF4 values were not increased, nor were there any changes seen in *Xbp1* splicing or eIF2α phosphorylation (see supplementary material, Figure S7). In contrast, there was a strong accumulation of the autophagy adaptor p62/SQSTM1 (hereafter referred to as p62) in double transgenic animals (Figure 5A) and a significant increase in PiZ mice compared with the non-transgenic ones (see supplementary material, Figure S8A,B). Immunostaining revealed a strong p62 signal in the cells accumulating both PiZ and HBs (Figure 5B,C). The p62 signal was particularly abundant in the vicinity of small AAT aggregates that are more common in the double transgenics (see supplementary material, Figure S8C). Double transgenic mice also displayed a significant increase in the autophagosomal membrane-associated form of LC3 (LC3-II) as well as in the LC3-II/LC3-I ratio, indicating an accumulation of autophagic vesicles (see supplementary material, Figure S8D,E). On the other hand, neither the LC3-II/b-actin ratio (not shown) nor LC3-II turnover assessed via a flux assay (see supplementary material, Figure S8F,G) was significantly altered among analyzed groups, suggesting that there is no obvious autophagic impairment. Despite that, the animals displayed signs of insufficient protein degradation. In particular, Z-HBs mice exhibited an accumulation of insoluble ubiquitinated proteins (see supplementary material, Figure S8H).

These findings prompted us to further evaluate the retention of both proteins in the autophagosomal/lysosomal compartment via gradient centrifugation. Z-HBs mice displayed a prominent AAT accumulation in both lysosomal and autophagosomal compartments, whereas HBs accumulated in the autophagosomal, but not in the lysosomal fraction of the double transgenic animals (Figure 5D). The purity of the analyzed fractions was

© 2021 The Authors. *The Journal of Pathology* published by John Wiley & Sons, Ltd. on behalf of The Pathological Society of Great Britain and Ireland. www.pathsoc.org

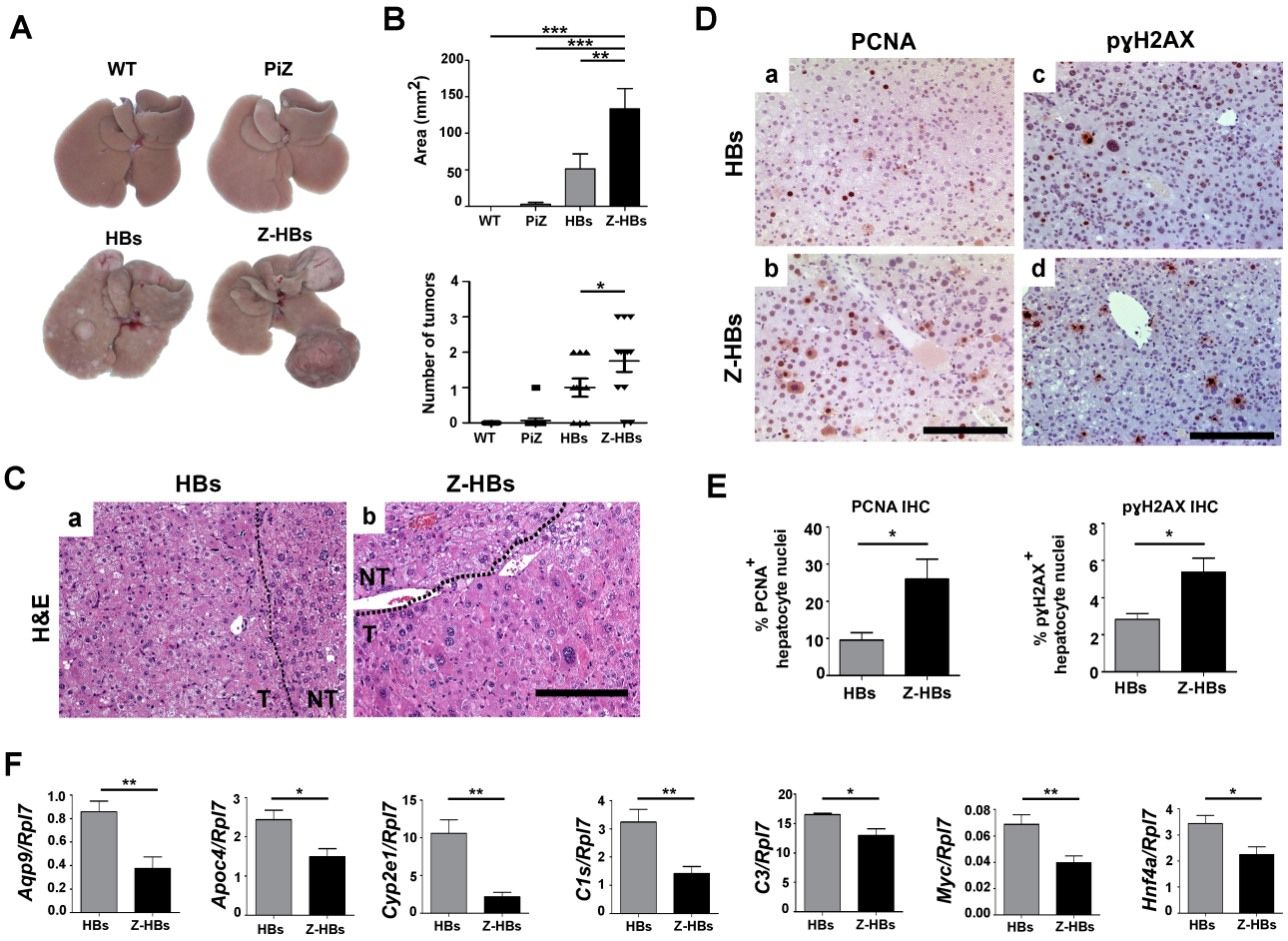


Figure 4. Dual proteotoxic stress leads to a higher tumor load and a more aggressive tumor subtype in Z-HBs mice. (A) Macroscopic appearance of livers from 14-month-old non-transgenics (WT), animals overexpressing PiZ variant of AAT (PiZ), HBs or both proteins together (Z-HBs). (B) Overall tumor load and tumor number are displayed as mean ± SEM (n = 11–12). (C) H&E staining (a,b) was carried out on representative liver sections, including tumor (T) and non-tumor (NT) areas, which are divided by dotted lines. Scale bar, 200 µm. (D) Proliferating hepatocytes and dysplastic cells were visualized in liver tumor sections by immunohistochemistry for PCNA (a,b) and pγH2AX (c,d) and the number of positive nuclei was quantified (mean ± SEM; n = 5) (E). Scale bar, 200 µm (Db,Dd). (F) Hepatic expression of the indicated genes in tumor tissues was examined by RT-qPCR (mean ± SEM; n = 7–10). *Aqp9*, Aquaporin; *Apoc4*, apolipoprotein 4; *Cyp2e1*, cytochrome P450, family 2, subfamily E, polypeptide 1; *C1s*, complement component 1, s subcomponent 1; *C3*, complement component 3; *Myc*, avian myeloblastosis virus oncogene cellular homolog; *Hnf4a*, hepatocyte nuclear factor 4 alpha. $^{*}p \leq 0.05$, $^{**}p \leq 0.01$, $^{***}p \leq 0.001$.

confirmed by immunoblotting (see supplementary material, Figure S9). To characterize the proteins interacting with p62, p62-containing particles were isolated with magnetic activated cell sorting separation (MACS). Immunoblotting demonstrated an accumulation of AAT, HBs, and Plin2 in double transgenic, but not in single transgenic littermates, thereby suggesting an overwhelmed aggrephagy (the degradation of misfolded proteins) and lipophagy (the degradation of lipids) in the Z-HBs animals (Figure 5E; supplementary material, Figure S10). Of note, immunoblotting of total lysates with characteristic ER and mitochondrial housekeeping genes did not show significant differences between the groups (see supplementary material, Figure S8I).

As p62 was described to promote tumor development due to activation of the Nrf2 pathway [32,33], Nrf2 activation was analyzed in 2-month-old animals. Z-HBs mice harbored higher Nrf2 levels in their nuclear fractions (Figure 6A,B) and an upregulation of the Nrf2 targets *Nqo1*, *Abcc4/Mrp4*, and *Hmox4* was noted (Figure 6C). As Nrf2 activation promotes survival of oxidatively damaged cells, we performed dihydroethidium (DHE) staining, which revealed significantly more DHE-positive cells in 10-month-old Z-HBs mice (Figure 6D,E).

Collectively, these data suggest that dual proteotoxic stress leads to a retention of proteins and activation of the p62–Nrf2 axis that promotes the development of liver disease and HCC (Figure 6F).

The presence of the PiZ variant predisposes CHB individuals to advanced liver fibrosis

To test whether the experimental findings suggesting the detrimental effects of dual proteotoxic stress translate to humans, we screened a large cohort of 830 patients with CHB for the presence of the PiZ variant (see supplementary material, Table S2). All patients gave a liver biopsy, which in 281 (34%) revealed advanced liver fibrosis (i.e. fibrosis stage 3/4). A heterozygous PiZ variant (PiMZ) was found in six individuals (allele frequency 0.4%); five of them

© 2021 The Authors. *The Journal of Pathology* published by John Wiley & Sons, Ltd. on behalf of The Pathological Society of Great Britain and Ireland. www.pathsoc.org

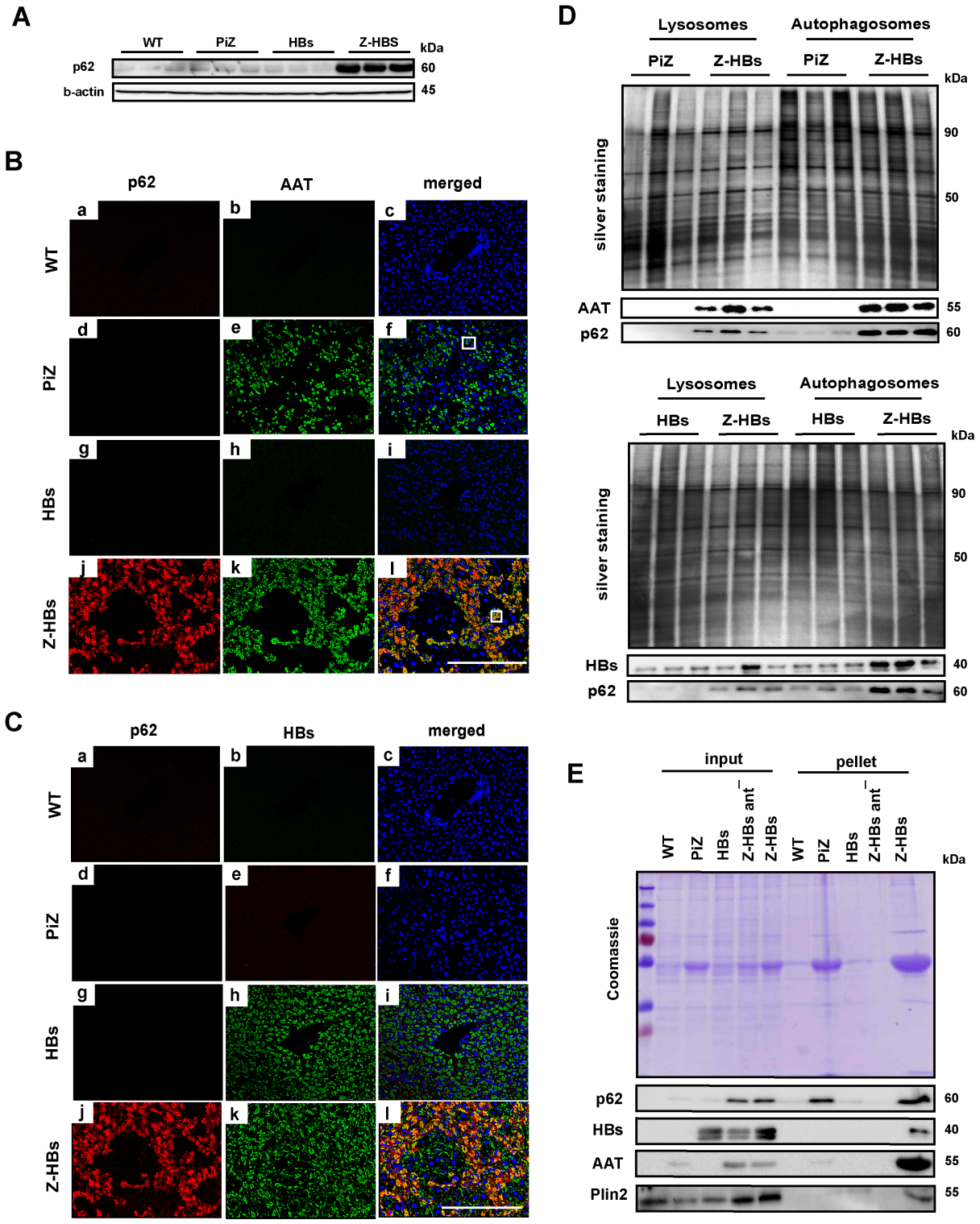


Figure 5. Dual proteotoxic stress leads to an accumulation of p62 and the other proteins in the degradatory pathway. (A) p62 protein levels were determined in total liver lysates by immunoblotting. b-actin was used as a loading control. Non-transgenic animals (WT), single transgenic mice overexpressing HBs (HBs) or PiZ variant of AAT (PiZ) were compared with the double transgenic Z-HBs mice. (B,C) Immunofluorescence staining for AAT (green), HBs (green) and p62 (red) was carried out on liver sections from the indicated mice. Nuclei were counterstained with DAPI (blue) and are visualized only in the merged images. The results were presented in two different panels to better capture the overlap between p62 (red) and AAT (green) (B) as well as p62 (red) and HBs (green) (C). The boxes in (Bf) and (Bl) highlight areas that are shown at greater magnification in supplementary material, Figure S8C. Scale bar, 200 μm (Bl) (Cl). (D) Lysosomal and autophagosomal fractions isolated from PiZ/Z-HBs (top) and from HBs/Z-HBs mice (bottom) were analyzed by immunoblotting. Silver staining was used as a loading control. (E) Immunoblots of p62-containing particles isolated from livers of the indicated experimental groups. The pull-down with beads only (ant–) served as a specificity control. Coomassie staining was used to visualize the isolated proteins.

© 2021 The Authors. *The Journal of Pathology* published by John Wiley & Sons, Ltd. on behalf of The Pathological Society of Great Britain and Ireland. www.pathsoc.org

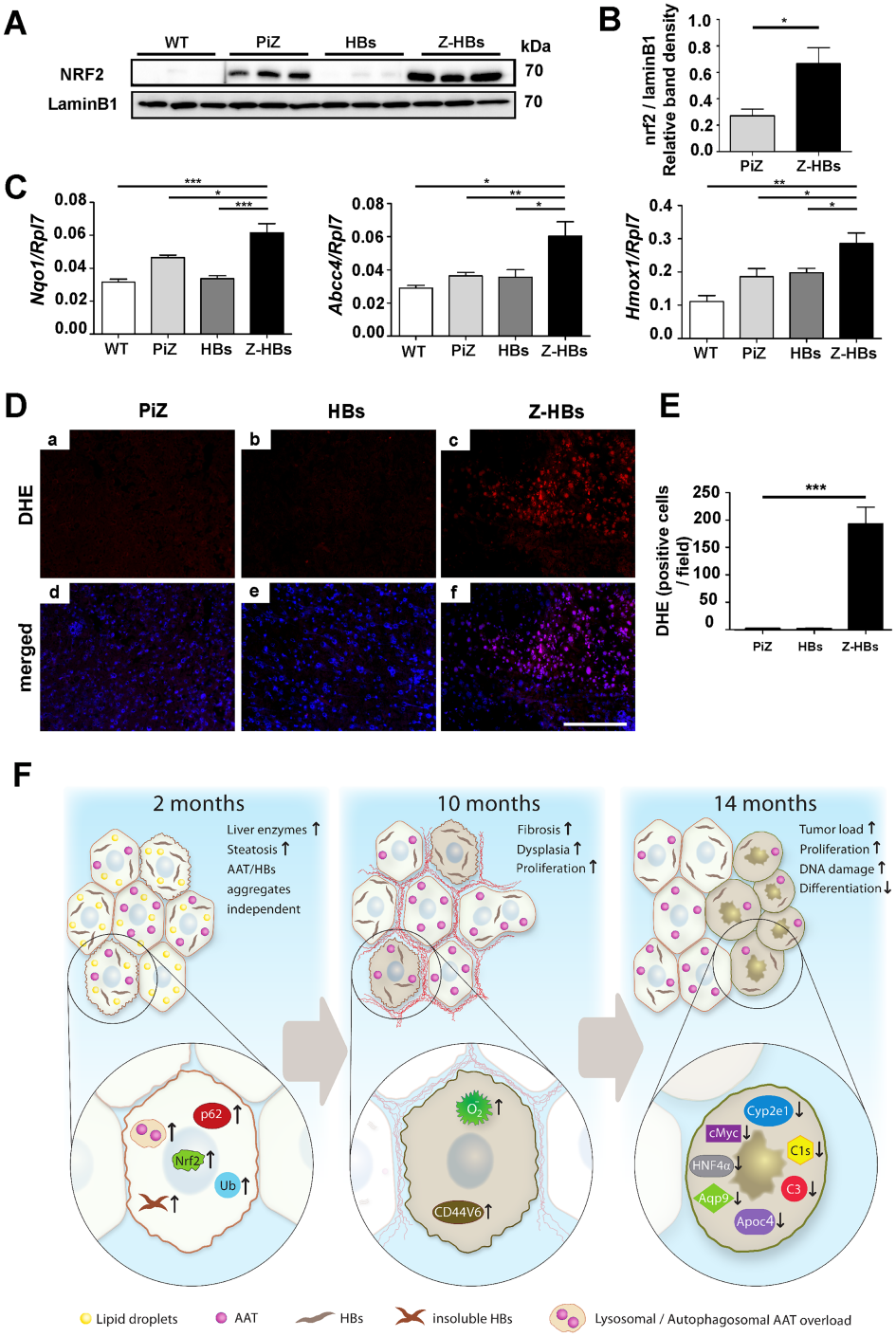


Figure 6. Double transgenic animals exhibit an activation of the Nrf2 pathway. (A) Immunoblotting of nuclear liver lysates from 2-month-old non-transgenic animals (WT), animals overexpressing PiZ variant of AAT (PiZ), HBs or both proteins (Z-HBs). Lamin B1 was used as a loading control. (B) Relative band density was quantified using ImageJ (mean ± SEM; $n = 3$). (C) Hepatic expression of various Nrf2 target genes was examined by RT-qPCR. Results are shown as mean ± SEM ($n = 5$–6) (D) DHE staining (red) of liver sections visualizes the level of reactive oxygen species in 10-month-old animals. Nuclei were stained with DAPI (blue). Scale bar, 200 µm. (E) Morphometric quantification of DHE-positive nuclei per field (mean ± SEM, $n \geq 5$). *$p \leq 0.05$, **$p \leq 0.01$, ***$p \leq 0.001$. (F) A schematic that summarizes the molecular alterations detected in Z-HBs mice. Only positive findings are depicted. Note that the highlighted molecular alterations were not studied in all age groups.

displayed advanced liver fibrosis. Accordingly, the presence of the PiZ variant was significantly associated with advanced liver fibrosis in the analyzed CHB cohort (odds ratio = 9.92 [1.15–85.39], $p = 0.04$ for F3–F4 versus F0–F2). Further studies are needed to delineate the impact of CHB on PiMZ individuals.

Discussion

In the present study, we analyzed the crosstalk between two paradigmatic hepatic proteotoxic conditions, i.e. HBs retention occurring in CHB and PiZ accumulation seen in AAT deficiency. The clinical relevance of this dual

© 2021 The Authors. *The Journal of Pathology* published by John Wiley & Sons, Ltd. on behalf of The Pathological Society of Great Britain and Ireland. www.pathsoc.org

proteotoxic stress was indicated by analysis of a large CHB cohort that revealed an over-representation of PiZ carriers among individuals with advanced liver fibrosis. These data support previous small-scale human studies implicating the PiZ variant as a disease-accelerating factor in CHB [17,34]; however, confirmatory studies are needed. Accordingly, we demonstrated that mice simultaneously overexpressing PiZ and HBs suffer from a more severe liver injury and an accelerated HCC development. This is in line with the current view that a dynamic interaction between the virus and the host shapes the development of CHB [35].

At first glance, both proteotoxic challenges seem to be fairly distinct, given that both proteins display an unrelated accumulation pattern and a different solubility in non-ionic detergents. The fact that HBs, but not AAT, strongly overlaps with calnexin suggests that the former is retained mainly in the corrective folding pathway, whereas PiZ accumulates in the downstream degradatory pathway. Although both HBs [36,37] and PiZ [38,39] undergo the calnexin–calreticulin folding attempt after their synthesis, our data suggest that PiZ needs more time to be digested after it is offloaded from the reparatory apparatus. This is not surprising, as polymerized, insoluble proteins such as PiZ are known to be difficult to degrade [2,40].

As detailed above, a greater production of aggregation-prone proteins challenges both the reparatory and degradatory pathways and may lead to their overload. Importantly, Z-HBs mice do not exhibit an unfolded protein response (which is activated via misfolded proteins with exposed hydrophobic residues) and are able to secrete a similar amount of both proteins as the single transgenes. In contrast, the degradatory capacity of the livers seems to be overwhelmed, as suggested by: (1) less pronounced co-localization of HBs with the calnexin and its translocation from the soluble to insoluble pool; (2) an overall increase in insoluble, ubiquitinated proteins; (3) retention of HBs/PiZ in the autophagosomal/lysosomal compartment coupled with an elevated LC3-II/LC3-I ratio; and (4) a greater amount of the autophagy adaptor p62. The dual proteotoxic stress in Z-HBs animals also results in markedly reduced PiZ inclusion size. In that respect, several authors have suggested that smaller aggregates rather than the mature inclusions probably constitute the toxic species. For example, a previous study demonstrated that an inability to form PiZ inclusion bodies leads to cell shrinkage and cell toxicity [38]. The same holds true for Huntington's disease, where the cells with smaller huntingtin assemblies were at higher risk of neural cell death [41–43].

To delineate the consequences of the overloaded degradatory pathway, we isolated p62-containing particles using MACS. Enrichment of AAT and HBs further substantiated an incomplete degradation of the surplus proteins, whereas retention of Plin2 may account for a reduced disposal of lipid droplets [30]. To that end, Plin2 is an established autophagy substrate and its degradation is a prerequisite for lipolysis [29,44]. Given the fact that hepatic steatosis is an important co-factor in the progression of liver disease and the development of HCC [45], future studies should explore the interaction between lipid metabolism and proteotoxic stress. Additional analyses are also needed to clearly delineate the impact of chronic proteotoxic stress on the different autophagic functions, such as mitophagy or ERphagy, as well as its impact on the ER.

With regard to other factors driving the development of liver injury/tumors in Z-HBs mice, the observed p62 accumulation probably plays a pivotal role, as p62 constitutes an important signaling hub promoting malignant transformation [33,46]. A critical mediator of p62-induced tumorigenesis detected in our double transgenic animals is the activation of Nrf2. Several studies report that p62 accumulation leads to the release of Nrf2 from Keap1, with its subsequent translocation into the nucleus [47,48]. Although Nrf2 is important in protection from oxidative stress, it also enables survival and malignant transformation of chronically stressed, oxidatively damaged cells [33,49,50]. In line with this, we observed an accumulation of these cells as well as decreased apoptosis rates in Z-HBs animals. Moreover, Nrf2 activation might be responsible for the higher proliferative rates in tumors from Z-HBs mice, as it regulates the metabolic response of cells, thereby favoring their proliferation [51,52]. Importantly, further studies are needed to delineate the precise mode of Nrf2 activation in our animals. Collectively, Z-HBs mice represent a novel tool to study the consequences of chronic ER protein overload in the liver and highlight the important role of p62 and Nrf2 in proteotoxic liver injury. Our data also demonstrate the need for novel treatment strategies targeting proteotoxic stress in patients who display progressive disease despite the treatment with nucleoside/nucleotide analogs. This is particularly relevant, as both PiZ and HBs retention can be easily targeted by RNA silencing approaches, and the corresponding clinical trials are entering clinical trials [53,54].

Acknowledgements

Our work was supported by a grant from the Interdisciplinary Centre for Clinical Research (IZKF) within the faculty of Medicine at the RWTH Aachen University, Else Kröner Exzellenzstipendium (to PS) and by the Deutsche Forschungsgemeinschaft (DFG) SFB TRR57 (to PS and CT) and STR1095/6-1 (to PS). ME and JG are supported by the Robert W. Storr Bequest to the Sydney Medical Foundation, University of Sydney; a National Health and Medical Research Council of Australia (NHMRC) Program Grant (1053206) and Project grants (APP1107178 and APP1108422). Open Access funding enabled and organized by Projekt DEAL.

Author contributions statement

DK and PS were responsible for the study concept and design, and drafted the manuscript. DK, KW, LS, AG,

© 2021 The Authors. *The Journal of Pathology* published by John Wiley & Sons, Ltd. on behalf of The Pathological Society of Great Britain and Ireland. www.pathsoc.org

GKE, YL, NGS, KH, RL, JH, JG, MM, ME, PL, AS, PN, SP, AM, TB, AB, WPB, MLA, AL. BS, HZ, CP and EA were responsible for the acquisition of data. DK, KW, GKE and JH analyzed and interpretated the data. DK and ME carried out the statistical analyses. PS obtained funding and supervised the study. DK, KW, LS, AG, GKE, YL, KK, NGS, KH, RL, JH, CT, JG, MM, ME, PL, SP, AM, TB, AB, WPB, MLA, AL, BS, HZ and EA provided technical or material support. All authors had access to the study data, critically reviewed the manuscript for important intellectual content, and approved the final manuscript.

References

1. Hartl FU. Protein misfolding diseases. *Annu Rev Biochem* 2017; **86:** 21–26.
2. Strnad P, Nuraldeen R, Guldiken N, *et al*. Broad spectrum of hepatocyte inclusions in humans, animals, and experimental models. *Compr Physiol* 2013; **3:** 1393–1436.
3. Kuscuoglu D, Janciauskiene S, Hamesch K, *et al*. Liver – master and servant of serum proteome. *J Hepatol* 2018; **69:** 512–524.
4. Wang M, Kaufman RJ. Protein misfolding in the endoplasmic reticulum as a conduit to human disease. *Nature* 2016; **529:** 326–335.
5. Madrigal-Matute J, Cuervo AM. Regulation of liver metabolism by autophagy. *Gastroenterology* 2016; **150:** 328–339.
6. Lomas DA, Hurst JR, Gooptu B. Update on alpha-1 antitrypsin deficiency: new therapies. *J Hepatol* 2016; **65:** 413–424.
7. Strnad P, McElvaney NG, Lomas DA. Alpha1-antitrypsin deficiency. *N Engl J Med* 2020; **382:** 1443–1455.
8. Teckman JH, Mangalat N. Alpha-1 antitrypsin and liver disease: mechanisms of injury and novel interventions. *Expert Rev Gastroenterol Hepatol* 2015; **9:** 261–268.
9. Blanco I, Bueno P, Diego I, *et al*. Alpha-1 antitrypsin Pi*SZ genotype: estimated prevalence and number of SZ subjects worldwide. *Int J Chron Obstruct Pulmon Dis* 2017; **12:** 1683–1694.
10. Greene CM, Marciniak SJ, Teckman J, *et al*. alpha1-antitrypsin deficiency. *Nat Rev Dis Primers* 2016; **2:** 16051.
11. Silverman EK, Sandhaus RA. Clinical practice. Alpha1-antitrypsin deficiency. *N Engl J Med* 2009; **360:** 2749–2757.
12. Hamesch K, Mandorfer M, Pereira VM, *et al*. Liver fibrosis and metabolic alterations in adults with alpha-1-antitrypsin deficiency caused by the Pi*ZZ mutation. *Gastroenterology* 2019; **157:** 705–719.e18.
13. Schneider CV, Hamesch K, Gross A, *et al*. Liver phenotypes of European adults heterozygous or homozygous for Pi *Z variant of AAT (Pi *MZ vs Pi *ZZ genotype) and noncarriers. *Gastroenterology* 2020; **159:** 534–548.e11.
14. Bartlett JR, Friedman KJ, Ling SC, *et al*. Genetic modifiers of liver disease in cystic fibrosis. *JAMA* 2009; **302:** 1076–1083.
15. Abul-Husn NS, Cheng X, Li AH, *et al*. A protein-truncating HSD17B13 variant and protection from chronic liver disease. *N Engl J Med* 2018; **378:** 1096–1106.
16. Strnad P, Buch S, Hamesch K, *et al*. Heterozygous carriage of the alpha1-antitrypsin Pi*Z variant increases the risk to develop liver cirrhosis. *Gut* 2019; **68:** 1099–1107.
17. Propst T, Propst A, Dietze O, *et al*. High prevalence of viral infection in adults with homozygous and heterozygous alpha 1-antitrypsin deficiency and chronic liver disease. *Ann Intern Med* 1992; **117:** 641–645.
18. Carlson JA, Rogers BB, Sifers RN, *et al*. Accumulation of PiZ alpha 1-antitrypsin causes liver damage in transgenic mice. *J Clin Invest* 1989; **83:** 1183–1190.
19. Hidvegi T, Ewing M, Hale P, *et al*. An autophagy-enhancing drug promotes degradation of mutant alpha1-antitrypsin Z and reduces hepatic fibrosis. *Science* 2010; **329:** 229–232.
20. European Association for the Study of the Liver. EASL 2017 Clinical practice guidelines on the management of hepatitis B virus infection. *J Hepatol* 2017; **67:** 370–398.
21. Ringelhan M, O'Connor T, Protzer U, *et al*. The direct and indirect roles of HBV in liver cancer: prospective markers for HCC screening and potential therapeutic targets. *J Pathol* 2015; **235:** 355–367.
22. Kawanaka M, Nishino K, Nakamura J, *et al*. Quantitative levels of hepatitis B virus DNA and surface antigen and the risk of hepatocellular carcinoma in patients with hepatitis B receiving long-term nucleos(t)ide analogue therapy. *Liver Cancer* 2014; **3:** 41–52.
23. Tseng TC, Liu CJ, Yang HC, *et al*. Serum hepatitis B surface antigen levels help predict disease progression in patients with low hepatitis B virus loads. *Hepatology* 2013; **57:** 441–450.
24. Chisari FV, Filippi P, McLachlan A, *et al*. Expression of hepatitis B virus large envelope polypeptide inhibits hepatitis B surface antigen secretion in transgenic mice. *J Virol* 1986; **60:** 880–887.
25. Chisari FV, Klopchin K, Moriyama T, *et al*. Molecular pathogenesis of hepatocellular carcinoma in hepatitis B virus transgenic mice. *Cell* 1989; **59:** 1145–1156.
26. Dunsford HA, Sell S, Chisari FV. Hepatocarcinogenesis due to chronic liver cell injury in hepatitis B virus transgenic mice. *Cancer Res* 1990; **50:** 3400–3407.
27. Bedossa P, Poynard T. An algorithm for the grading of activity in chronic hepatitis C. The METAVIR Cooperative Study Group. *Hepatology* 1996; **24:** 289–293.
28. Guldiken N, Kobazi Ensari G, Lahiri P, *et al*. Keratin 23 is a stress-inducible marker of mouse and human ductular reaction in liver disease. *J Hepatol* 2016; **65:** 552–559.
29. Kaushik S, Cuervo AM. Proteostasis and aging. *Nat Med* 2015; **21:** 1406–1415.
30. Kaushik S, Cuervo AM. Degradation of lipid droplet-associated proteins by chaperone-mediated autophagy facilitates lipolysis. *Nat Cell Biol* 2015; **17:** 759–770.
31. Romualdo GR, Grassi TF, Goto RL, *et al*. An integrative analysis of chemically-induced cirrhosis-associated hepatocarcinogenesis: histological, biochemical and molecular features. *Toxicol Lett* 2017; **281:** 84–94.
32. Duran A, Amanchy R, Linares JF, *et al*. p62 is a key regulator of nutrient sensing in the mTORC1 pathway. *Mol Cell* 2011; **44:** 134–146.
33. Umemura A, He F, Taniguchi K, *et al*. p62, upregulated during preneoplasia, induces hepatocellular carcinogenesis by maintaining survival of stressed HCC-initiating cells. *Cancer Cell* 2016; **29:** 935–948.
34. Hashemi M, Alavian SM, Ghavami S, *et al*. High prevalence of alpha 1 antitrypsin phenotypes in viral hepatitis B infected patients in Iran. *Hepatol Res* 2005; **33:** 292–297.
35. Trépo C, Chan HL, Lok A. Hepatitis B virus infection. *Lancet* 2014; **384:** 2053–2063.
36. Norton PA, Menne S, Sinnathamby G, *et al*. Glucosidase inhibition enhances presentation of de-N-glycosylated hepatitis B virus epitopes by major histocompatibility complex class I in vitro and in woodchucks. *Hepatology* 2010; **52:** 1242–1250.
37. Prange R, Werr M, Löffler-Mary H. Chaperones involved in hepatitis B virus morphogenesis. *Biol Chem* 1999; **380:** 305–314.
38. Granell S, Baldini G, Mohammad S, *et al*. Sequestration of mutated alpha1-antitrypsin into inclusion bodies is a cell-protective mechanism to maintain endoplasmic reticulum function. *Mol Biol Cell* 2008; **19:** 572–586.
39. Liu Y, Choudhury P, Cabral CM, *et al*. Intracellular disposal of incompletely folded human alpha1-antitrypsin involves release from calnexin and post-translational trimming of asparagine-linked oligosaccharides. *J Biol Chem* 1997; **272:** 7946–7951.

© 2021 The Authors. *The Journal of Pathology* published by John Wiley & Sons, Ltd. on behalf of The Pathological Society of Great Britain and Ireland. www.pathsoc.org

40. Kaganovich D, Kopito R, Frydman J. Misfolded proteins partition between two distinct quality control compartments. *Nature* 2008; **454:** 1088–1095.
41. Arrasate M, Mitra S, Schweitzer ES, *et al*. Inclusion body formation reduces levels of mutant huntingtin and the risk of neuronal death. *Nature* 2004; **431:** 805–810.
42. Soares TR, Reis SD, Pinho BR, *et al*. Targeting the proteostasis network in Huntington's disease. *Ageing Res Rev* 2019; **49:** 92–103.
43. Yang J, Hao X, Cao X, *et al*. Spatial sequestration and detoxification of Huntingtin by the ribosome quality control complex. *Elife* 2016; **5:** e11792.
44. Tsai TH, Chen E, Li L, *et al*. The constitutive lipid droplet protein PLIN2 regulates autophagy in liver. *Autophagy* 2017; **13:** 1130–1144.
45. Font-Burgada J, Sun B, Karin M. Obesity and cancer: the oil that feeds the flame. *Cell Metab* 2016; **23:** 48–62.
46. Moscat J, Diaz-Meco MT. p62 at the crossroads of autophagy, apoptosis, and cancer. *Cell* 2009; **137:** 1001–1004.
47. Komatsu M, Kurokawa H, Waguri S, *et al*. The selective autophagy substrate p62 activates the stress responsive transcription factor Nrf2 through inactivation of Keap1. *Nat Cell Biol* 2010; **12:** 213–223.
48. Bartolini D, Dallaglio K, Torquato P, *et al*. Nrf2-p62 autophagy pathway and its response to oxidative stress in hepatocellular carcinoma. *Transl Res* 2018; **193:** 54–71.
49. Nakagawa H, Umemura A, Taniguchi K, *et al*. ER stress cooperates with hypernutrition to trigger TNF-dependent spontaneous HCC development. *Cancer Cell* 2014; **26:** 331–343.
50. Sakurai T, He G, Matsuzawa A, *et al*. Hepatocyte necrosis induced by oxidative stress and IL-1 alpha release mediate carcinogen-induced compensatory proliferation and liver tumorigenesis. *Cancer Cell* 2008; **14:** 156–165.
51. DeNicola GM, Chen PH, Mullarky E, *et al*. NRF2 regulates serine biosynthesis in non-small cell lung cancer. *Nat Genet* 2015; **47:** 1475–1481.
52. Mitsuishi Y, Taguchi K, Kawatani Y, *et al*. Nrf2 redirects glucose and glutamine into anabolic pathways in metabolic reprogramming. *Cancer Cell* 2012; **22:** 66–79.
53. NCT03945292. Safety, tolerability and effect on liver histologic parameters of ARO-AAT. Available from: https://ClinicalTrials.gov/show/NCT03945292. [Accessed 5 March 2020].
54. NCT03772249. Study of safety and tolerability of DCR HBVS. Available from: https://ClinicalTrials.gov/show/NCT03772249. [Accessed 5 March 2020].
55. Kant S, Holthöfer B, Magin TM, *et al*. Desmoglein 2-dependent arrhythmogenic cardiomyopathy is caused by a loss of adhesive function. *Circ Cardiovasc Genet* 2015; **8:** 553–563.
56. Lunova M, Goehring C, Kuscuoglu D, *et al*. Hepcidin knockout mice fed with iron-rich diet develop chronic liver injury and liver fibrosis due to lysosomal iron overload. *J Hepatol* 2014; **61:** 633–641.
57. Wattiaux R, Wattiaux-De Coninck S, Ronveaux-dupal MF, *et al*. Isolation of rat liver lysosomes by isopycnic centrifugation in a metrizamide gradient. *J Cell Biol* 1978; **78:** 349–368.
58. Janciauskiene S, Dominaitiene R, Sternby NH, *et al*. Detection of circulating and endothelial cell polymers of Z and wild type alpha 1-antitrypsin by a monoclonal antibody. *J Biol Chem* 2002; **277:** 26540–26546.

References 55–58 are cited only in the supplementary material.

SUPPLEMENTARY MATERIAL ONLINE

Supplementary materials and methods

Figure S1. Two-month-old Z-HBs mice display no significant changes in body or liver weight or in lipid serum parameters

Figure S2. Double transgenic animals display a translocation of HBs into an insoluble pool

Figure S3. Differing accumulation patterns of AAT and HBs in Z-HBs mice

Figure S4. Ten-month-old double transgenics showed elevated liver transaminases and an increased liver-to-body weight ratio

Figure S5. Fourteen-month-old double transgenic animals display a marked elevation of liver injury parameters and an increased liver-to-body weight ratio

Figure S6. The tumors arising in animals overexpressing HBs and animals overexpressing both the PiZ variant of AAT and HBs (Z-HBs) resemble well-differentiated HCC

Figure S7. The simultaneous presence of AAT and HBs does not lead to ER stress

Figure S8. Z-HBs mice display signs of an overloaded degradatory pathway

Figure S9. Gradient centrifugation results in pure subcellular fractionation

Figure S10. Z-HBs mice display a protein retention in the degradatory pathway

Table S1. Characteristics of the cohort of patients used for molecular analysis

Table S2. Characteristics of the cohort of patients with CHB screened for the presence of the PiZ variant in the AAT gene

Table S3. Histopathological evaluation of H&E-stained liver sections from 2-month-old mice

Table S4. Histopathological evaluation of tumors dissected from HBs and Z-HBs mice

Table S5. Antibodies used for immunoblotting and immunohistochemistry

Table S6. Primers for genotyping and RT-qPCR

© 2021 The Authors. *The Journal of Pathology* published by John Wiley & Sons, Ltd. on behalf of The Pathological Society of Great Britain and Ireland. www.pathsoc.org

Dual proteotoxic stress accelerates liver injury via activation of p62-Nrf2

D Kuscuoglu *et al. J Pathol* DOI: 10.1002/path.5643

Supplementary materials and methods

Reference numbers refer to the main text list

Tissue staining

For immunofluorescence (IF), Oil Red O (ORO) and dihydroethidium (DHE) staining, liver pieces were embedded in Tissue-Tek Compound (Sakura, Osaka, Japan), snap frozen and cut into 5 µm thick frozen sections. The sections were incubated for IF staining with the indicated primary antibodies (supplementary material, Table S5) overnight at +4 °C. After washing with Tris buffered saline containing 0.1% Tween (1x TBST), the appropriate fluorescent dye-conjugated secondary antibodies (Life Technologies GmbH, Darmstadt, Germany) were applied (supplementary material, Table S5).

The presence of reactive oxygen species (ROS) was determined by dihydroethidium staining (DHE) (Thermo Fisher Scientific, Schwerte, Germany). In brief, air dried specimens were incubated with 5 µM DHE solution for 15 min at 37 °C and were washed with 1x PBS to remove the excess dye. For IF and DHE staining, mounting medium containing 4′,6-diamidino-2-phenylindole (DAPI, Life Technologies, Invitrogen, Germany) was used to counterstain the nuclei. The signal was analyzed either using a Leica DM5500B fluorescence light microscope (Leica Microsystems GmbH, Wetzlar, Germany) or a confocal laser scanning microscope (LSM 710 DUO, Zeiss, Jena, Germany).

To visualize the lipids, ORO staining was performed. Air dried sections were fixed with 10% formalin for 5 min at room temperature (RT) and afterwards washed briefly with running tap water.

Next, liver samples were rinsed with 60% isopropanol (Sigma-Aldrich, St. Louis, Missouri, USA) and incubated in fresh ORO working solution for 15 min at RT. The excess, unbound dye was removed with 60% isopropanol. Counterstaining was carried out by incubation of the slides in 1:10 diluted hematoxylin solution (1:1 diluted with water, Roth, Karlsruhe, Germany). The slides were covered with aqueous Kaiser's glycerol gelatin (Merck, Darmstadt, Germany). Bright red colored lipid droplets were evaluated using a Zeiss light microscope (ImagerA2, Zeiss, Göttingen, Germany) and the area of lipid was quantified using ImageJ software.

For immunohistochemical (IHC) or histological staining, liver sections were placed overnight in 4% formaldehyde solution, dehydrated, embedded in paraffin and cut into 5 µm thick sections. IHC was performed using the Vectastain ABC Systems Reagents (Vector Laboratories, Burlingame, CA) and antibodies specific for AAT (A11, Euro Diagnostica, Malmö, Sweden), HBs (SIG-3433, Covance, Princeton, NJ, USA), PCNA (MS106P, ThermoScientific, Waltham, MA, USA) and pγH2AX (9718, Cell Signaling Technology, Danvers, MA, USA). Immunodetection was carried out with vector Nova Red Kit (Vector Laboratories) after labeling with species-specific biotin-conjugated secondary antibodies (supplementary material, Table S5).

Electron microscopy (EM)

Transmission electron microscopy was done as described [55]. Liver tissues were cut into small pieces (~ 1 mm^3) before being subjected to a three-step fixation process. First, they were treated with EM fixative solution (3.7% formaldehyde, 1% glutaraldehyde, 11.6 g $NaH_2PO_4 \cdot H_2O$, and 2.7 g NaOH per liter of ddH_2O) for 2 h at RT and then with 1% OsO_4 for 1 h. Lastly, they were incubated in EM contrast solution (0.5% uranyl actetate in 0.05 M sodium maleate buffer) for 2 h at RT. The samples were then dehydrated and embedded in araldite for 48 h at 60 °C with acetone. They were then cut into 75 nm ultrathin sections and subsequently treated with 3% uranyl acetate for 4 min then 80 mM lead citrate for 3 min to further enhance the contrast. Electron micrographs were obtained using an EM 10 (Zeiss) microscope equipped with a digital camera (Olympus) and iTEM software (Olympus).

RT-qPCR analysis

Total RNA was isolated from liver tissue samples using an RNeasy Mini Kit (Qiagen, Hilden, Germany) according to the kit manual. Reverse transcription into cDNA was carried out using an M-MLV-Reverse-Transcriptase Kit (Promega, Mannheim, Germany). Quantitative real time PCR was performed using a 7300 Fast Real Time PCR system (Applied Biosystems, Foster City, CA, USA) using SYBR Green-containing master mix (Applied Biosystems, Schwerte, Germany) and specific primers (supplementary material, Table S6). Transcripts of the mouse ribosomal protein gene *Rpl7* were used as an internal reference. All real-time PCR reactions were performed in duplicate and the mean of expression data (Ct values) was used to calculate the relative expression of target gene compared to *Rpl7*.

Protein analysis

Total liver lysates were prepared in a homogenization buffer containing 3% sodium dodecyl sulfate (SDS: Roth). To divide the proteins based on their solubility in non-ionic detergents, 1% Triton X containing buffer was used and the pellets were dissolved with 3% SDS-containing buffer. For subcellular fractionation, the livers were homogenized in 0.25 M sucrose buffer and the fractions were obtained as described [56,57]. p62-containing particles were collected using magnetic activated cell sorting separation (MACS) according to the manufacturer's instructions (Miltenyi biotec., Bergisch Gladbach, Germany). In brief, frozen liver tissue was homogenized in 1x PBS supplemented with a proteinase inhibitor PefaBloc (Roche, Mannheim, Germany) and the tissue was disrupted with stainless steel beads in a TissueLyser II (Qiagen, Hilden, Germany). Homogenates were filtered through a 100 µm polyamide membrane (Klein Wieler, Königswinter, Germany) then centrifuged at 25 000 x *g* for 10 min at 4 °C. The pellet was resuspended in 1x PBS/proteinase inhibitor buffer and incubated with the primary antibody against p62 (PM045, MBL, Sunnyvale, CA, USA). After incubation, the pellet was suspended in 400 µl MACS buffer and was incubated with 30 µl MACS anti-rabbit IgG Microbeads at 4 °C for 30 min on a tube rotator (VWR, Radnor, PA, USA). The suspension was loaded to activated MACS LS columns 25

(Miltenyi biotec.) which were placed into MACS Quadro Separator (Miltenyi biotec.). After a short washing step, the column was removed from the separator, and the magnetically labeled particles were eluted from the column with the appropriate buffer. The particles were pelleted at 25 000 x *g* for 10 min at 4 °C and were kept at -80 °C until used. Samples incubated with beads without an antibody served as a specificity control.

The isolated protein extracts were diluted in 4× reducing Laemmli buffer and the proteins were separated by 8–10% SDS–polyacrylamide gel electrophoresis. Electrophoresed proteins were either visualized by Coomassie or silver staining, or were transferred to PVDF membranes for immunoblotting. After the transfer, the blots were incubated with the appropriate primary and secondary antibodies, the latter being conjugated with horseradish peroxidase (HRP) (supplementary material, Table S5). The labeled proteins were visualized using enhanced chemiluminescence (Prime Western Blotting Detection Reagents, GE Healthcare, Chicago, IL, USA). The resulting light emission was detected by a luminescent image analyzer ImageQuant LAS 4000 (GE Healthcare).

Biochemical assays

Hepatic hydroxyproline levels were measured as described [56]. In brief, frozen liver tissues were hydrolyzed in 6 M hydrogen chloride (HCl) at 110 °C for 18 h. The homogenates were filtered through Macherey-Nagel filters (55 µm, Macherey-Nagel, Düren, Germany) and dried by vacuum centrifugation (Eppendorf AG, Hamburg, Germany). The pellets and trans-4-hydroxy-L-proline standards (Sigma, Rödermark, Germany) were dissolved in 50% isopropanol, and mixed with 0.6% chloramine-T oxidation solution for 10 min at RT in order to oxidize free hydroxyproline to pyrrole. Fresh Ehrlich's solution was added to obtain chromophores and the absorbance of pyrrole-based chromophores was measured at wavelength of 570 nm using an ELISA Reader µQuant (BioTek, Winooski, VT, USA) equipped with KC4 Software. Hydroxyproline content was normalized to wet liver weight and was presented as mg/g (hydroxyproline amount/wet liver weight).

To analyze the extent of lipid accumulation, small pieces of frozen liver tissue were placed into 500 µl ethanolic KOH and incubated overnight at 55 °C in a water bath (VWB18, VWR). The resulting liver homogenates were mixed with EtOH/H_2O (1:1) solution and centrifuged at 14 000 rpm for 5 min at 4 °C. Next, $MgCl_2$ (1 M, 215 µl) was mixed with the supernatant (200 µl). The mixture was incubated on ice for 10 min and was centrifuged at 14 000 rpm for 5 min at 4 °C. The amount of triglyceride in supernatants was measured in the Clinical Chemistry Department of the University Hospital Aachen. The normalization was done according to wet liver weight and was presented as mg/g (triglyceride amount/wet liver weight).

LC3 flux assay

To analyze the autophagic flux an *ex vivo* LC3 flux assay was performed. Mice were sacrificed, blood was removed, and 500 mg liver tissue was cut into small pieces. These were evenly divided into two parts and transferred to 1.5 ml Williams medium E (P04-29510, PAN-Biotech GmbH, Aidenbach, Germany) supplemented with FCS 10%. For autophagy inhibition, 200 µM leupeptin and 20 mM NH_4Cl were added to one part of the minced tissue and the suspensions were incubated at 37 °C with moderate shaking for 3.5 h. After the incubation, the mixtures were centrifuged at 16 000 x *g* for 10 min at 4 °C. The supernatant was discarded, the pellet was washed with ice-cold 1x PBS and homogenized in homogenization buffer with 3% sodium dodecyl sulfate (SDS, Roth) using stainless steel beads in a TissueLyser II. The homogenate was heated at 95 °C for 5 min and centrifuged at 14 000 rpm for 2 min at RT. The supernatant was diluted in 4x reducing Laemmli buffer and the samples were analyzed using 15% SDS–PAGE, carried out as described above. Densitometry analyses were performed using ImageJ and the amount of LC3-II relative to actin used as a loading control was determined.

Dual proteotoxic stress accelerates liver injury via activation of p62-Nrf2

D Kuscuoglu *et al. J Pathol* DOI: 10.1002/path.5643

Supplementary Figures S1–S10

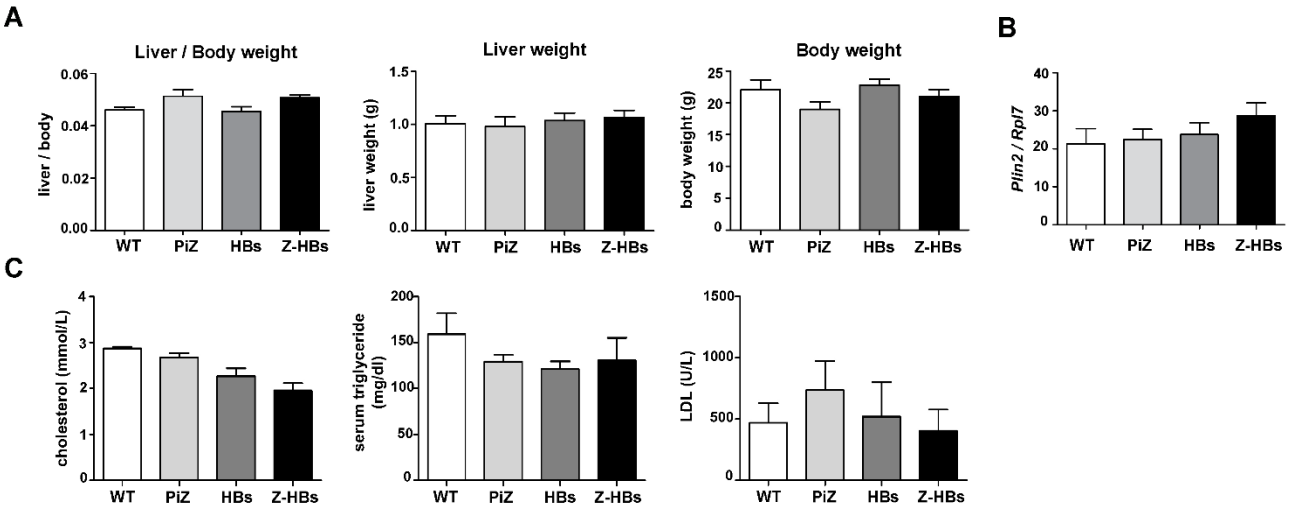


Figure S1. Two-month-old Z-HBs mice display no significant changes in body or liver weight or in lipid serum parameters. (A) The body and liver weight were measured in non-transgenic animals (WT), animals overexpressing the PiZ variant of AAT (PiZ), HBs or both proteins (Z-HBs) and the data were presented as mean ± SEM (*n* = 5–10). (B) Hepatic expression of *Plin2* (Perilipin 2) relative to the housekeeping gene *Rpl7* was examined by RT-qPCR. Results are shown as mean ± SEM (*n* = 5). (C) The concentrations of cholesterol, triglyceride, and low-density lipoprotein cholesterol (LDL) in serum were also determined (mean ± SEM, *n* = 5).

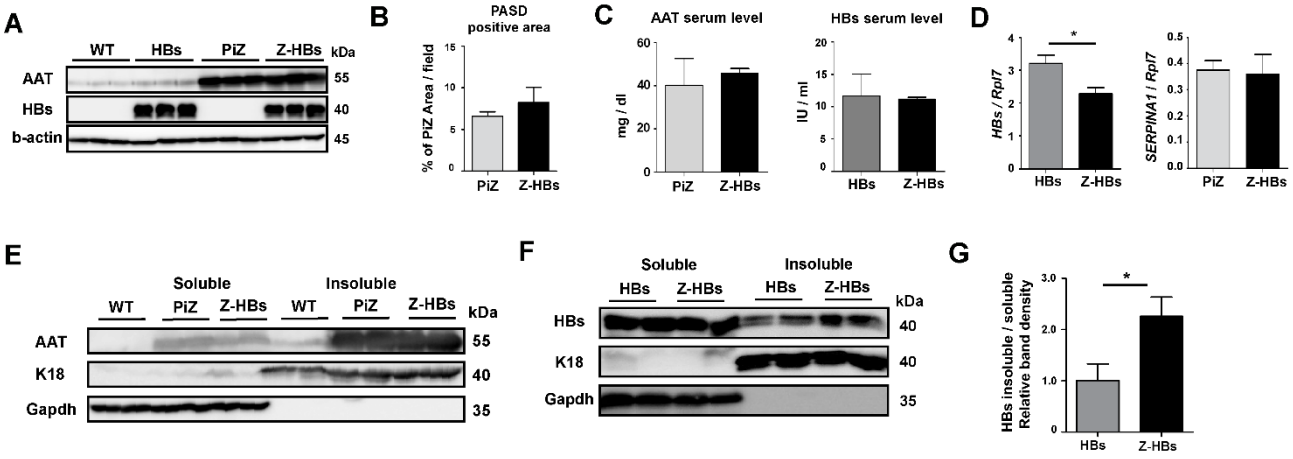


Figure S2. Double transgenic animals display a translocation of HBs into an insoluble pool. (A) Immunoblotting assessed the amount of AAT and HBs in total liver lysates from non-transgenic animals as well as mice overexpressing the PiZ variant of AAT (PiZ), HBs or both proteins together (Z-HBs). b-actin was used as loading control. (B) Graph indicates the periodic acid-Schiff diastase (PASD) positive area quantified by morphometric analysis of histological liver sections (mean ± SEM; *n* = 5). (C) Serum AAT and HBs levels are shown as mean ± SEM (*n* = 5). (D) Hepatic expression of *HBs* and *Serpina1a* relative to the housekeeping gene *Rpl7* was examined by RT-qPCR (mean ± SEM; *n* = 4). **p* ≤ 0.05. (E,F) Liver proteins were separated into soluble and insoluble fractions using 1% Triton X buffer and immunoblotting against the indicated antigens was performed. Gapdh and Keratin 18 (K18) were used as soluble and insoluble loading controls, respectively. (G) The relative amount of HBs in insoluble versus soluble protein pool was quantified using ImageJ (mean ± SEM; *n* = 3) **p* ≤ 0.05.

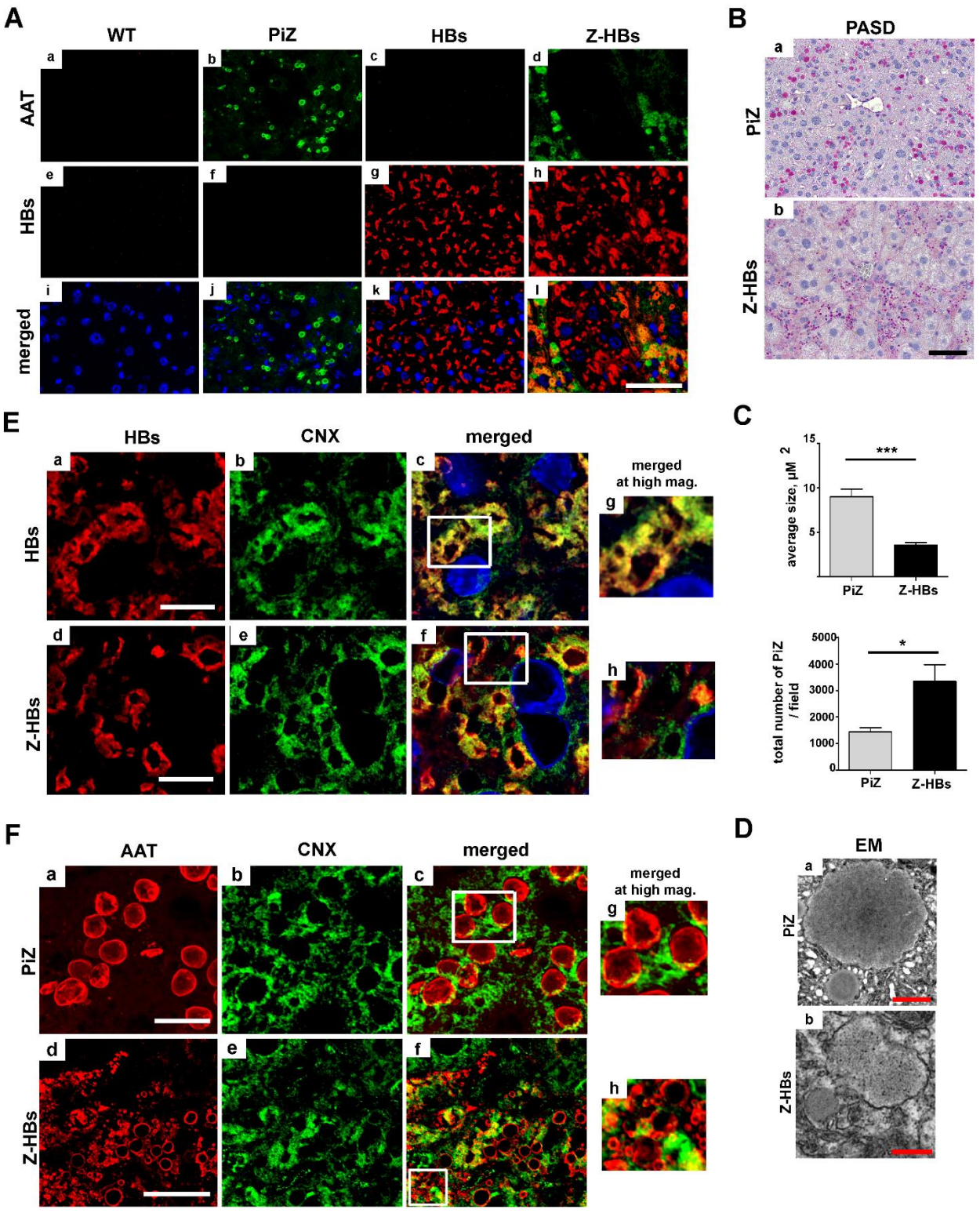


Figure S3. Differing accumulation patterns of AAT and HBs in Z-HBs mice. (A) Immunofluorescence staining (IF) reveals the distribution of AAT (a–d) and HBs (e–h) as

well as the overlap of both signals (i–l). Scale bar = 50 µm. (B,C) Periodic acid-Schiff diastase staining (PASD) visualizes PiZ aggregates that were further quantified by morphometric analysis (mean ± SEM; n = 5). Scale bar: 25 µm (b). (D) Representative electron micrographs demonstrate a similar AAT aggregate ultrastructure in PiZ and Z-HBs mice. Scale bar: 1 µm (PiZ), 0.25 µm (Z-HBs). Confocal image stacks of liver sections stained for (E) HBs and calnexin (CNX) or (F) for AAT and CNX. Nuclei were stained with DAPI (blue). To highlight the overlap between the signals, selected areas from merged images (indicated by boxes) are shown at greater magnification. Scale bar: 10 µm. *$p \leq 0.05$, ***$p \leq 0.001$.

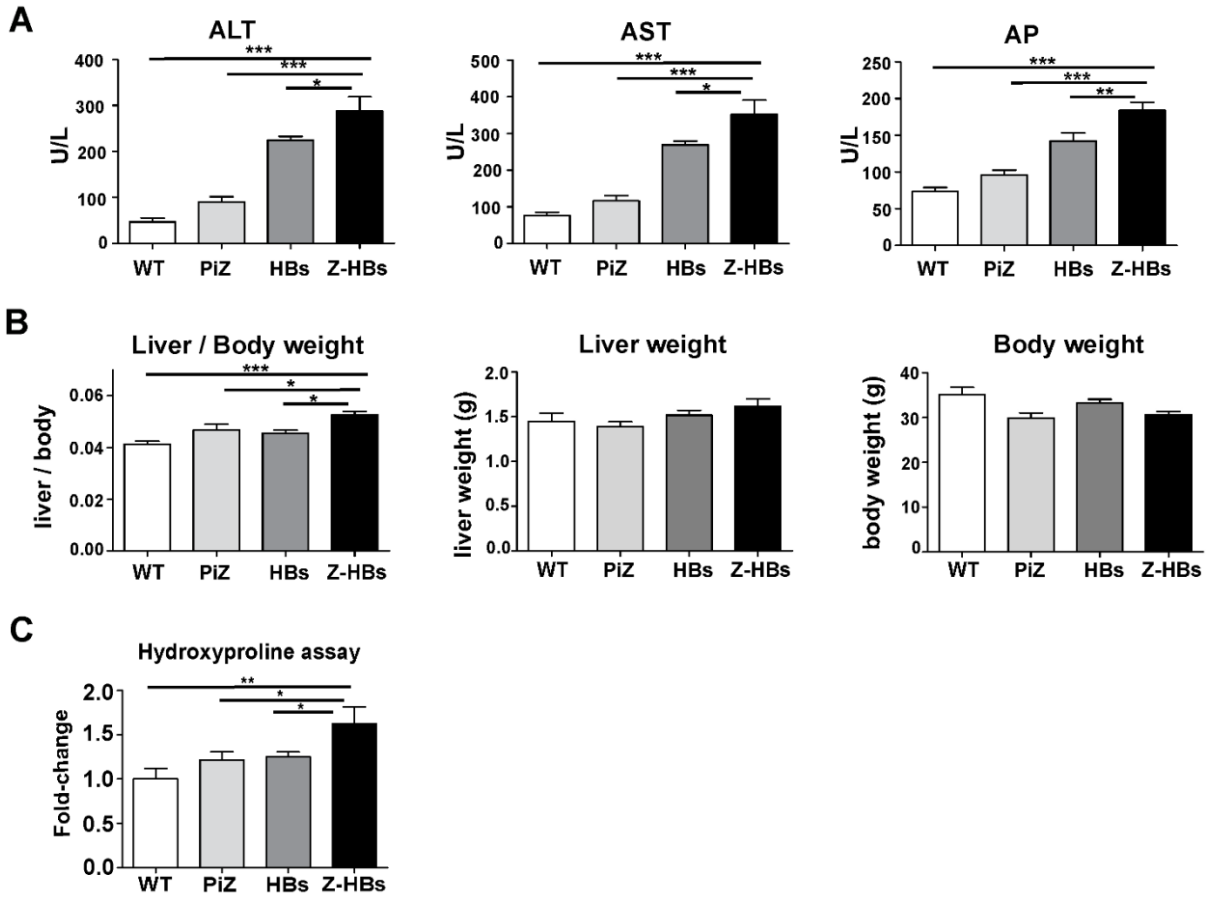


Figure S4. Ten-month-old double transgenics showed elevated liver transaminases and an increased liver-to-body weight ratio. (A) Graphs indicate the levels of serum alanine aminotransferase (ALT), aspartate aminotransferase (AST), and alkaline phosphatase (AP) in 10-month-old non-transgenic animals (WT), animals overexpressing the PiZ variant of AAT (PiZ), HBs or both proteins (Z-HBs). The data are expressed as mean ± SEM and at least six samples per group were used. (B) Liver and body weight as well as the liver-to-body weight ratio were determined (mean ± SEM; n = 6). (C) Hepatic hydroxyproline levels were assessed in liver lysates from the indicated, age-matched littermates (mean ± SEM; n = 10). *$p \leq 0.05$, **$p \leq 0.01$, ***$p \leq 0.001$.

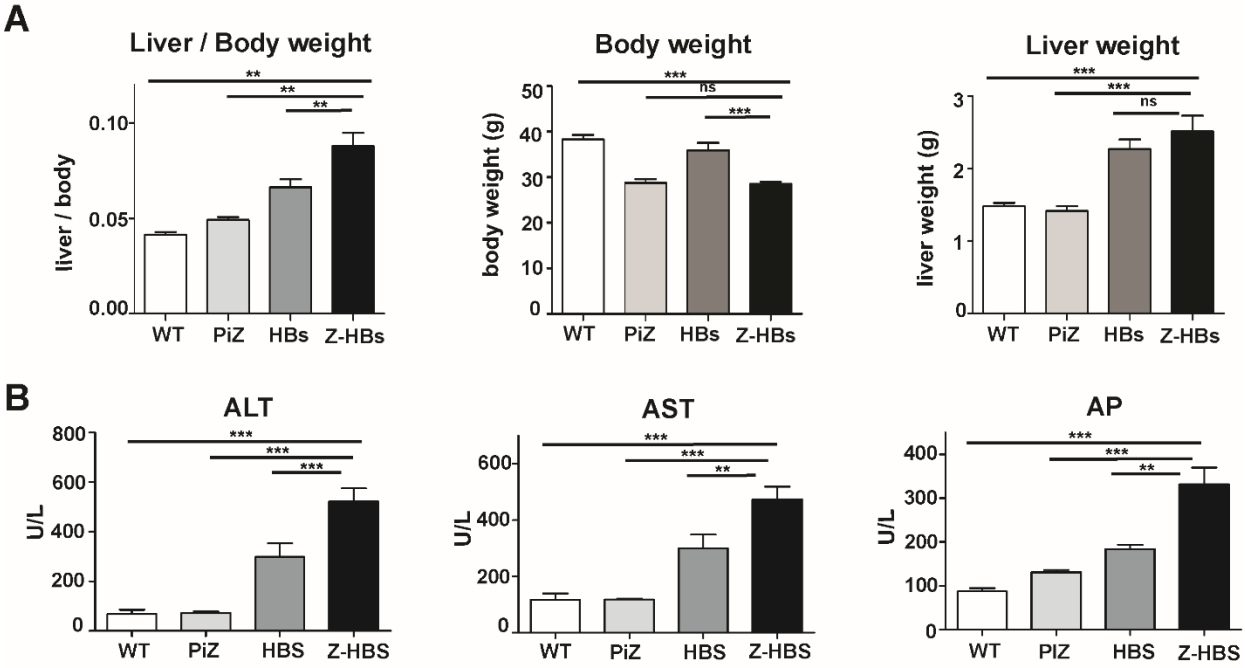


Figure S5. Fourteen-month-old double transgenic animals display a marked elevation of liver injury parameters and an increased liver-to-body weight ratio. (A) Graphs display liver and body weight as well as liver-to-body weight ratio in non-transgenic animals (WT), animals overexpressing the PiZ variant of AAT (PiZ), HBs or both proteins (Z-HBs). Mean ± SEM; *n* = 11–12. (B) Measurement of alanine aminotransferase (ALT), aspartate aminotransferase (AST), and alkaline phosphatase (AP) serum levels was carried out for the indicated genotypes (mean ± SEM; *n* = 8). ***p* ≤ 0.01, ****p* ≤ 0.001.

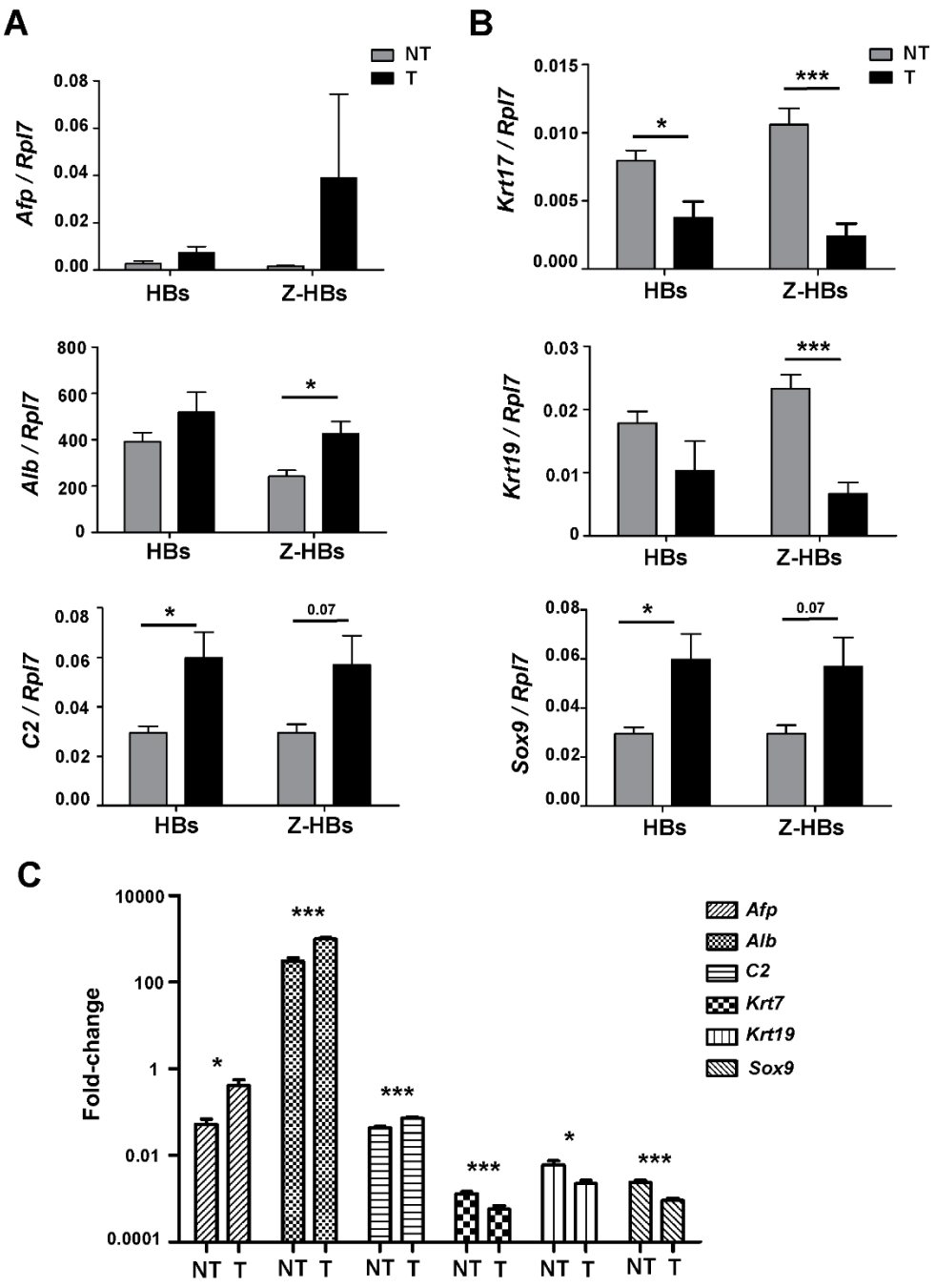


Figure S6. The tumors arising in animals overexpressing HBs and animals overexpressing both the PiZ variant of AAT and HBs (Z-HBs) resemble well-differentiated HCC. The hepatic mRNA levels of selected markers of (A) hepatocellular and (B) cholangiocellular lineage were analyzed in non-transgenic animals (WT), animals overexpressing the PiZ variant of AAT (PiZ), HBs or both proteins (Z-HBs) by RT-qPCR.

Results are shown as mean ± SEM (*n* = 7–10). (C) Hepatic expression of the same genes was examined in well-characterized mouse model of well-differentiated HCC induced by a combined treatment with diethylnitrosamine and carbon tetrachloride by RT-qPCR (mean ± SEM; *n* = 7–11). The relative expression was quantified and *Rpl7* was used as a reference transcript. **p* ≤ 0.05, ***p* ≤ 0.01, ****p* ≤ 0.001. NT, non-tumorous tissue; T, tumorous tissue; *Afp*, alpha-fetoprotein; *Alb*, albumin; *C2*, complement component 2; *Krt7*, keratin 7; *Krt19*, keratin 19; *Sox9*, SRY (sex determining region Y)-box 9.

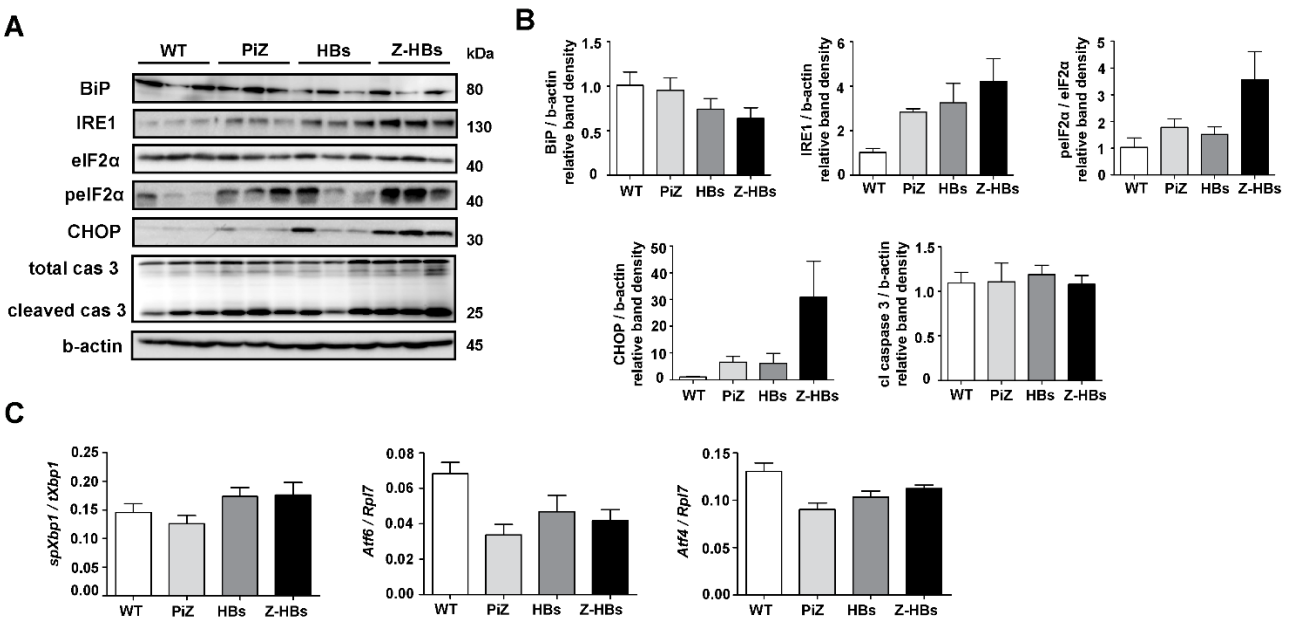


Figure S7. The simultaneous presence of AAT and HBs does not lead to ER stress. (A) Immunoblotting assessed the amount of indicated proteins in total liver lysates from non-transgenic animals (WT), animals overexpressing the PiZ variant of AAT (PiZ), HBs or both proteins (Z-HBs). b-actin was used as loading control. (B) The relative band density was quantified using ImageJ (mean ± SEM; *n* = 6). (C) Hepatic expression of various ER stress-related genes was examined by RT-qPCR. The ratio of total (t) and spliced (sp) isoform of the X-box binding protein 1 (*Xbp1*) was quantified. Results are shown as mean ± SEM (*n* = 5–6).

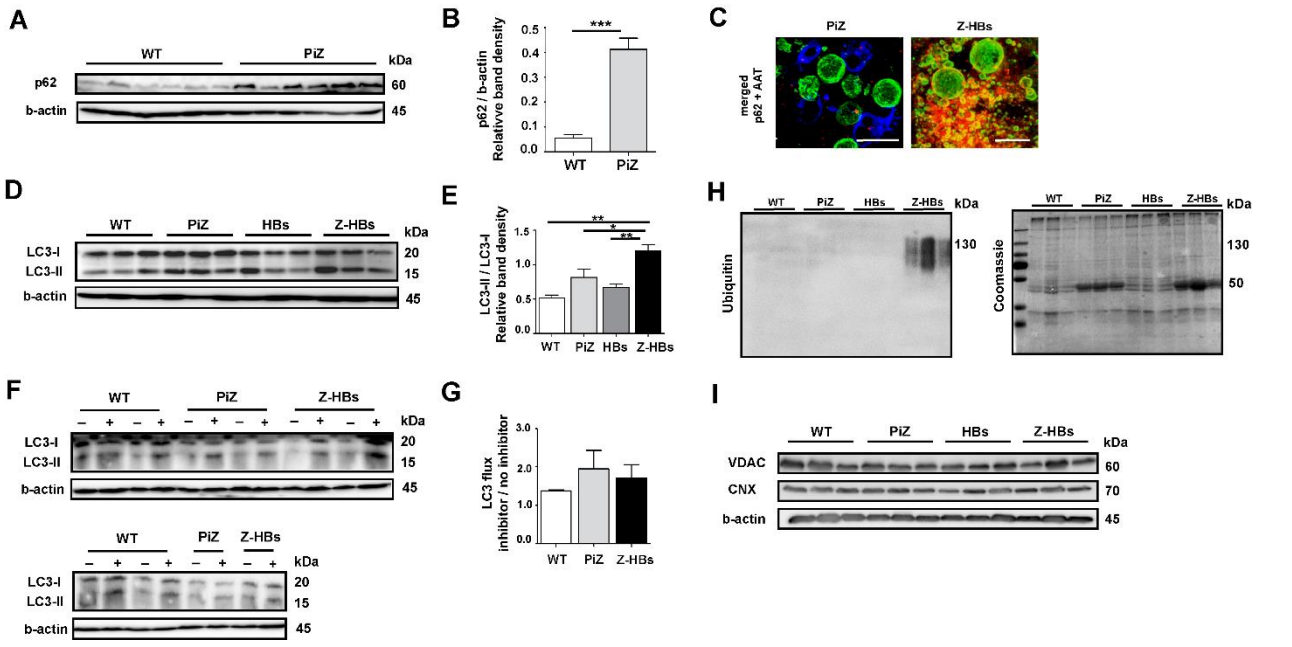


Figure S8. Z-HBs mice display signs of an overloaded degradatory pathway. (A) p62 protein levels were determined in total liver lysates by immunoblotting. Non-transgenic animals (WT) as well as mice overexpressing the PiZ variant of AAT (PiZ) were analyzed and b-actin was used as a loading control. (B) The relative band density was quantified using ImageJ (mean ± SEM; *n* = 6). (C) Double immunofluorescence staining (IF) for AAT (green) and p62 (red) was performed on liver sections. The images provide greater magnifications using laser scanning microscopy of the regions marked in Figure 5B. Scale bar = 10 µm (PiZ) (Ca), 5 µm (Z-HBs) (Cb). (D,E) Total liver lysates from non-transgenic animals as well as mice overexpressing the PiZ variant of AAT (PiZ), HBs or both proteins together (Z-HBs) were analyzed by immunoblotting and the relative band density of LC3-II compared to LC3-I was quantified using ImageJ (mean ± SEM; *n* = 3). b-actin was used as a loading control. (F,G) An autophagy flux assay was performed and assessed LC3-II levels (relative to actin as a loading control) in presence or absence of the autophagy inhibitor. The

ratios between the relative LC3-II levels in presence or absence of the autophagy inhibitor was calculated for each animal. The graph displays average LC3-II ratios in the individual genotypes (mean ± SEM; *n* = 3). (H) Immunoblot analysis of 1% Triton X insoluble liver fractions. Coomassie staining was used to show loading. (I) Immunoblot analysis of 1% Triton X-insoluble liver fractions. Coomassie staining was used to show loading. CNX, calnexin; VDAC, voltage-dependent anion-selective channel.

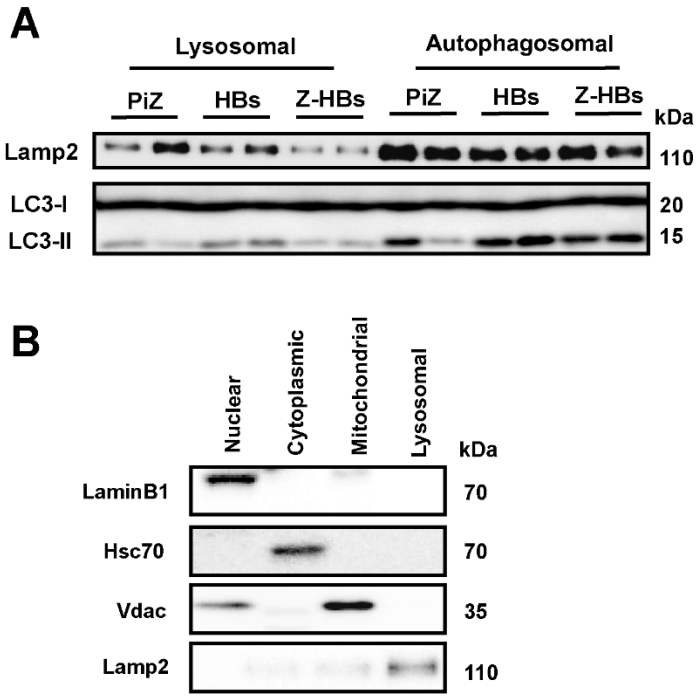


Figure S9. Gradient centrifugation results in pure subcellular fractionation. (A) Autophagosomal and lysosomal fractions were obtained from livers of transgenic mice overexpressing the PiZ variant of AAT (PiZ), HBs or both proteins together (Z-HBs) and subjected to immunoblotting against the indicated proteins. (B) An example of subcellular fractionation of a liver from wild-type mouse. Immunoblotting was used to confirm the purity of the different fractions. Vdac, voltage-dependent anion-selective channel.

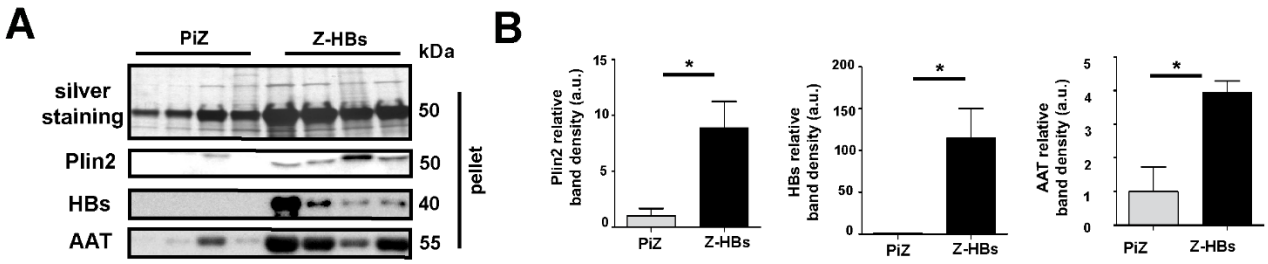


Figure S10. Z-HBs mice display a protein retention in the degradatory pathway.

(A,B) p62-containing particles isolated from livers of PiZ and Z-HBs mice were subjected to immunoblotting with subsequent quantification of band density. The average band density in PiZ mice was arbitrarily set as 1 and the amounts in double transgenic mice represent a ratio. *$p \leq 0.05$, **$p \leq 0.01$.